# CHAPTER V

# RESULTS AND DISCUSSION

In this chapter, the results and discussion are divided into five sections. The formation of pure metal oxide are presented in section 5.1. In section 5.2, the effect of solvent and reaction temperature on the crystallite size of titanium (IV) oxide, iron (III) oxide and zinc (II) oxide are presented. The formation of silicon modified metal oxide are presented in section 5.3. Section 5.4, the effect of silicon on the crystallite size of metal oxide product are concluded. In the last section, the effect of silicon on thermal stability of these metal oxides are explained.

## 5.1 Formation of pure metal oxide

### 5.1.1 Formation of titanium (IV) oxide and the effect of reaction temperature on titanium (IV) oxide product

The nanocrystal titanium (IV) oxide (titania) obtained in this work were synthesized from titanium tert-butoxide (TNB) mixed with organic solvents; 1,4-butanediol or toluene at various reaction temperatures under autogeneous pressure. The procedure is so-call solvothermal method. Titania prepared in each organic solvent have different physical properties and thermal stability.



#### 5.1.1.1 Reaction in 1,4 butanediol



Reaction of titanium tert-butoxide in 1,4-butanediol at various reaction temperatures, Glycothermal Method. Under glycothermal conditions, titanium (IV) tert-butoxide was easily converted to glycoxide. Thermal decomposition of the glycoxide molecule was occurred by intramolecular participation of the remaining hydroxyl group of glycol moiety and subsequently a $\equiv Ti\text{-}O^-$ anion was formed. The nucleophilic attack of this titanate ion on another ion and crystallization of titanium (IV) oxide were taken place. The mechanism of TNB in 1,4-BG can be depicted in Figure 5.1

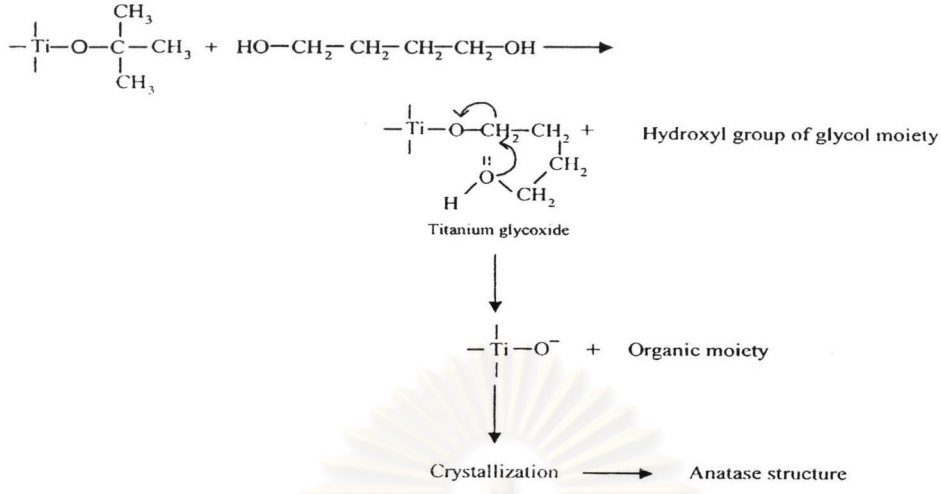


**Figure 5.1** Mechanism of glycothermal reaction for the anatase formation (Sornnarong Theinkeaw, 2000:70).

The nanocrystal titanium (IV) oxide were synthesized by reaction in 1,4-BG at various reaction temperatures (200, 230, 250, 270, 300, 320 and 340°C) for 2 hours under autogeneous pressure. The XRD patterns of the as-synthesized product obtained from glycothermal reaction is given in Figure 5.2, which shows that the synthesized titania product at 200°C appeared amorphous phase indicated that TNB was not hydrolized and remain in the solvent. At 230°C, hydrolysis of TNB completely proceeded to yield a poorly crystallized anatase phase. When the reaction temperature was raised to 250°C, the intensity of the peaks for the anatase phase increased with increased in crystallite size.

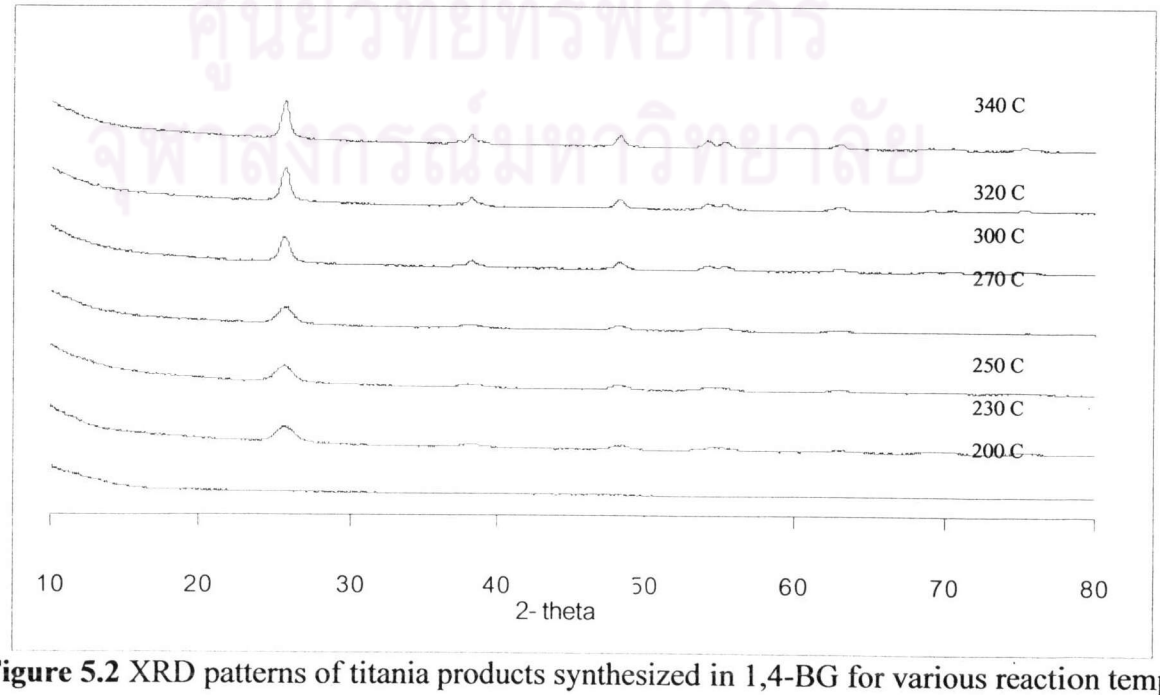


**Figure 5.2** XRD patterns of titania products synthesized in 1,4-BG for various reaction temperatu

Table 5.1 shows the crystallite sizes calculated from XRD patterns at 101 diffraction peak of the anatase titania by Scherrer equation (Kominami et al., 1997; Yang et al., 2001; Iwamoto et al., 2001) and the specific surface area of titania which is measured by two methods. The first method is the specific surface area BET measurement ($S_1$) and the other is the specific surface area calculated from equation of $6/d\rho$ on assumption that the crystal is nonporous spherical crystal ($S_2$). For the reaction temperature of 230°C, the crystallite size and BET surface area of the as-synthesized product were 5.9 nm and 163.2 $m^2/g$, respectively and the surface area which was calculated from diameter size of the crystal become 240.9 $m^2/g$. When the reaction temperature was increased, the crystallite size gradually increased but the surface area decreased.

It should be noted that the growth of anatase crystal gradually proceeded in the present reaction medium on the contrary to the glycothermal treatment (Kominami et al. 1999). Interestingly, the obtained surface area was different from BET surface area with the small crystallite synthesized by lower temperature but when the reaction temperature was increased (increased in crystallite size) the calculated surface area was not different from BET surface area. These identify that the titania product is not contaminate with amorphous-like phase or organic phase as shown through ratio of $S_1/S_2$. Kominami et al. (1997) synthesized titania from the solvothermal method. They calculated the surface area from the crystallite size by assuming the density of anatase to be 3.84 $gcm^{-3}$. They found that the surface area obtained from BET measurement was larger than that calculated from the crystallite size and suggested that the product was contaminated with the amorphous-like phase.

The titania products were characterized by SEM for analyzing morphology of the products as shown in Figure 5.3 SEM results indicated that morphology of the secondary particle which a shape was irregular particle is not change with increasing the reaction temperature.

**Table 5.1** Crystallite size and surface area of titanium (IV) oxide products synthesized in 1,4-BG at different reaction temperature.

| Reaction Temperature (°C) | Crystallite size (nm) | Surface area ($m^2/g$) | | $S_1/S_2$ |
|---|---|---|---|---|
| | | $S_1$[a] | $S_2$[b] | |
| 200 | amorphous | - | - | - |
| 230 | 5.9 | 163.2 | 240.9 | 0.7 |
| 250 | 6.2 | 163.9 | 230.8 | 0.7 |
| 270 | 7.3 | 145.3 | 196.8 | 0.7 |
| 300 | 12.9 | 123.9 | 110.4 | 1.1 |
| 320 | 14.2 | 95.2 | 100.4 | 0.9 |
| 340 | 15.4 | 83.3 | 92.5 | 0.9 |

[a]Specific BET surface area from BET measurement

[b]Specific surface area calculated from equation of $6/d\rho$ on assumption that the crystal is nonporous spheres and using the density of anatase of 4.2 $g/cm^3$

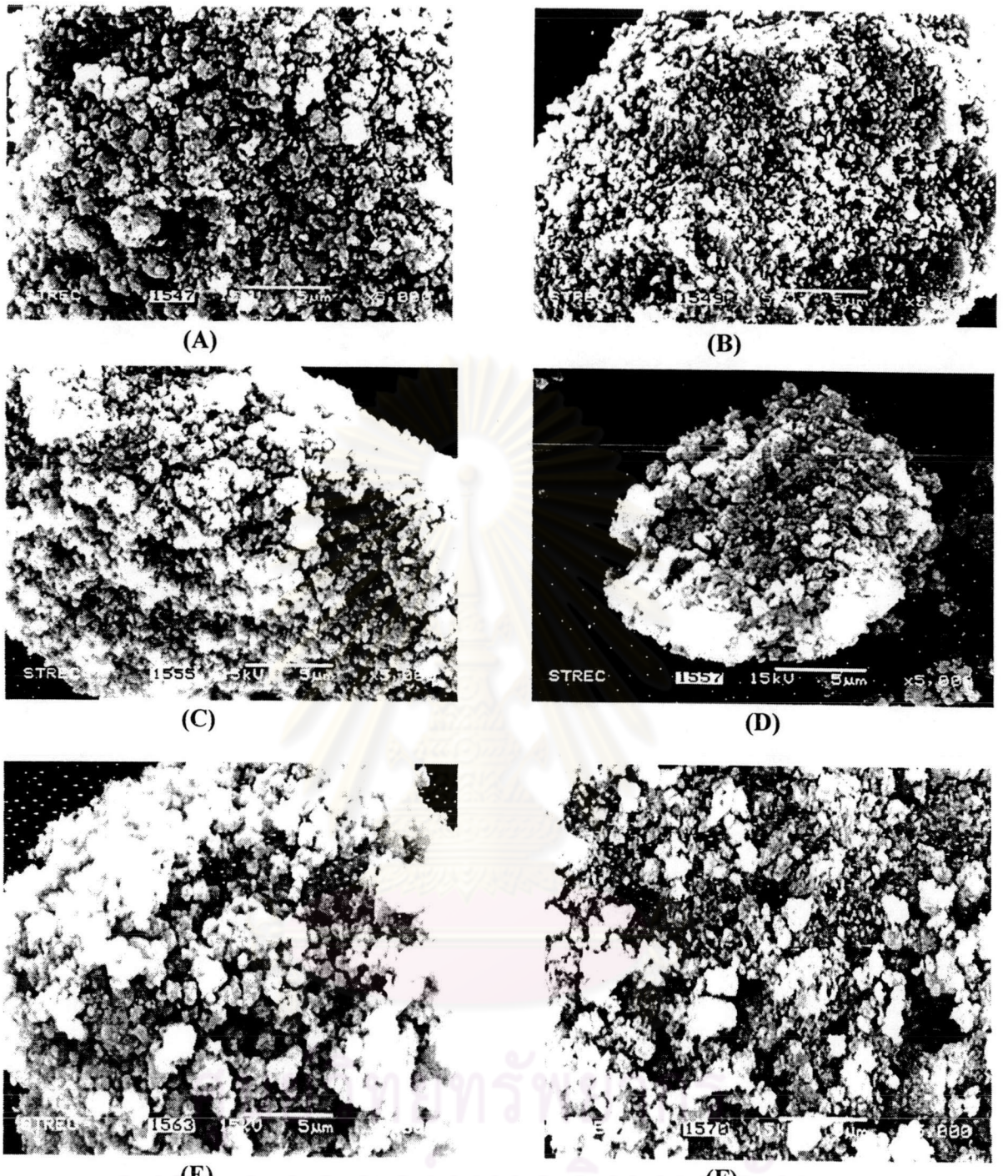


**Figure 5.3** SEM morphology of titania products synthesized in 1,4-BG for various reaction temperatures (A) 230°C, (B) 250°C, (C) 270°C, (D) 300°C, (E) 320°C, and (F) 340°C.

### 5.1.1.2 Reaction in toluene

Titanium (IV) oxide has been synthesized in toluene at various reaction temperatures (Solvothermal Method). In this work the effect of reaction temperature was investigated. Under inert organic solvent condition, thermal decomposition of TNB in toluene was occurred, yielding a ≡ Ti-$O^-$ anion. The nucleophilic attack of the titanate ion on the another ion and crystallization was taken place, finally yielding the anatase titania. The mechanism of TNB in toluene can be depicted as follow.

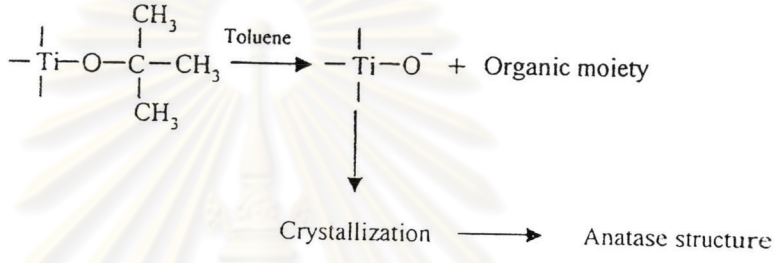


**Figure 5.4** Mechanism of reaction in toluene for the titania product.

Titania was synthesized in toluene for various reaction temperatures (250, 270, 300, 320, and 340°C). As shown in Figure 5.5, XRD pattern of the products synthesized at 250°C, appeared amorphous phase but for raising the temperature to 270°C, titania products started to become anatase without contamination of other phase such as rutile and brookite, which denoted that titania product was formed at these temperature.

Kominami et al. (1999) synthesized titanium (IV) oxide by hydrolysis of titanium (IV) alkoxide in toluene with water that was dissolved from the gas phase at high temperature. When the reaction was carried out at 125°C, TNB was not hydrolyzed and remained in the solvent with elevated the reaction temperature to 150° C, hydrolysis of TNB completely proceeded to yield a poorly crystalized anatase titania. When the reaction temperature was raised to 300°C, the crystallite size increased. Kondo et al. (1994) examined the hydrothermal treatment of alkoxide-derived amorphous $TiO_2$ particles and found that the crystallite size of anatase formed was increased to 25 nm by the treatment at 250°C

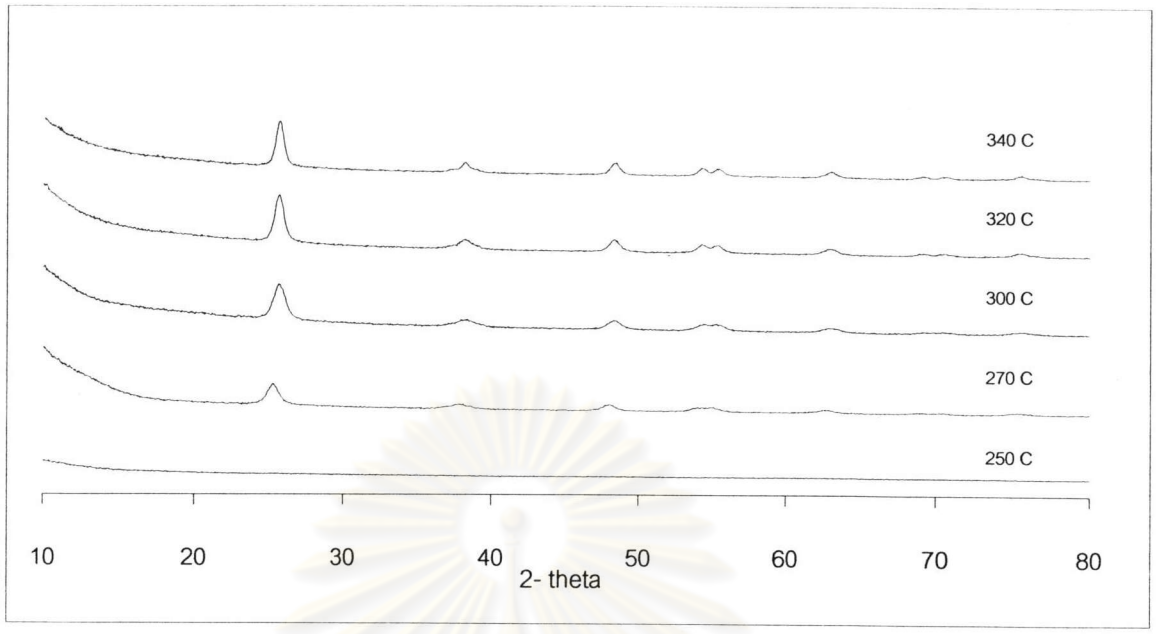


**Figure 5.5** XRD patterns of titania products synthesized in toluene for various reaction temperatures.

From XRD pattern, the crystallite size of the anatase was calculated from the half-height width of the 101 diffraction peak of anatase using the Scherrer equation. The crystallite size synthesized at 270°C was 8.9 nm and approached 14 nm at 340°C as shown in Table 5.2.

Table 5.2 shows the crystallite size and specific surface area. The crystallite size increased slightly with increasing the reaction temperature. Considering the same crystallite size, it was found that a decrease of the surface area indicated the product contaminated with amorphous form was changed to crystal form. On the other hand, the specific surface areas obtained from both BET measurement and calculation was decreased with increasing the reaction temperature. It can be concluded that the reaction temperature has an influence on the nucleation of crystal.

Considering $S_1/S_2$ values, which compared the BET surface areas with surface areas that calculated from crystallite size. The values were increased with increasing the reaction temperature, indicated that the products were possibly formed to the single crystal or free-flow crystal, a crystal formed by the growth of a crystal nucleus

**Table 5.2** Crystallite size and surface area of titanium (IV) oxide product synthesized in toluene at different reaction temperature.

| Reaction Temperature (°C) | Crystallite size (nm) | Surface area ($m^2/g$) | | $S_1/S_2$ |
|---|---|---|---|---|
| | | $S_1$[a] | $S_2$[b] | |
| 250 | amorphous | - | - | - |
| 270 | 8.9 | 140.0 | 160.7 | 0.9 |
| 300 | 8.9 | 128.5 | 160.7 | 0.8 |
| 320 | 12.9 | 109.6 | 110.4 | 1.0 |
| 340 | 14.2 | 70.1 | 100.4 | 0.7 |

[a]Specific BET surface area from BET measurement

[b]Specific surface area calculated from equation of $6/d\rho$ on assumption that the crystal is nonporous spheres and using the density of anatase of 4.2 $g/cm^3$

without secondary nucleation or impingement on other crystal. However, with the reaction temperature was 340°C, the crystal was not the single crystal so that the $S_1/S_2$ value is less than unity.

SEM image as seen in Figure 5.6 reveals that the anatase titania tends to agglomerated to secondary particles in spherical shape. The secondary particles morphology from SEM show the formation of spherical shape, not only being a large size but also agglomerating with increasing the reaction temperature.

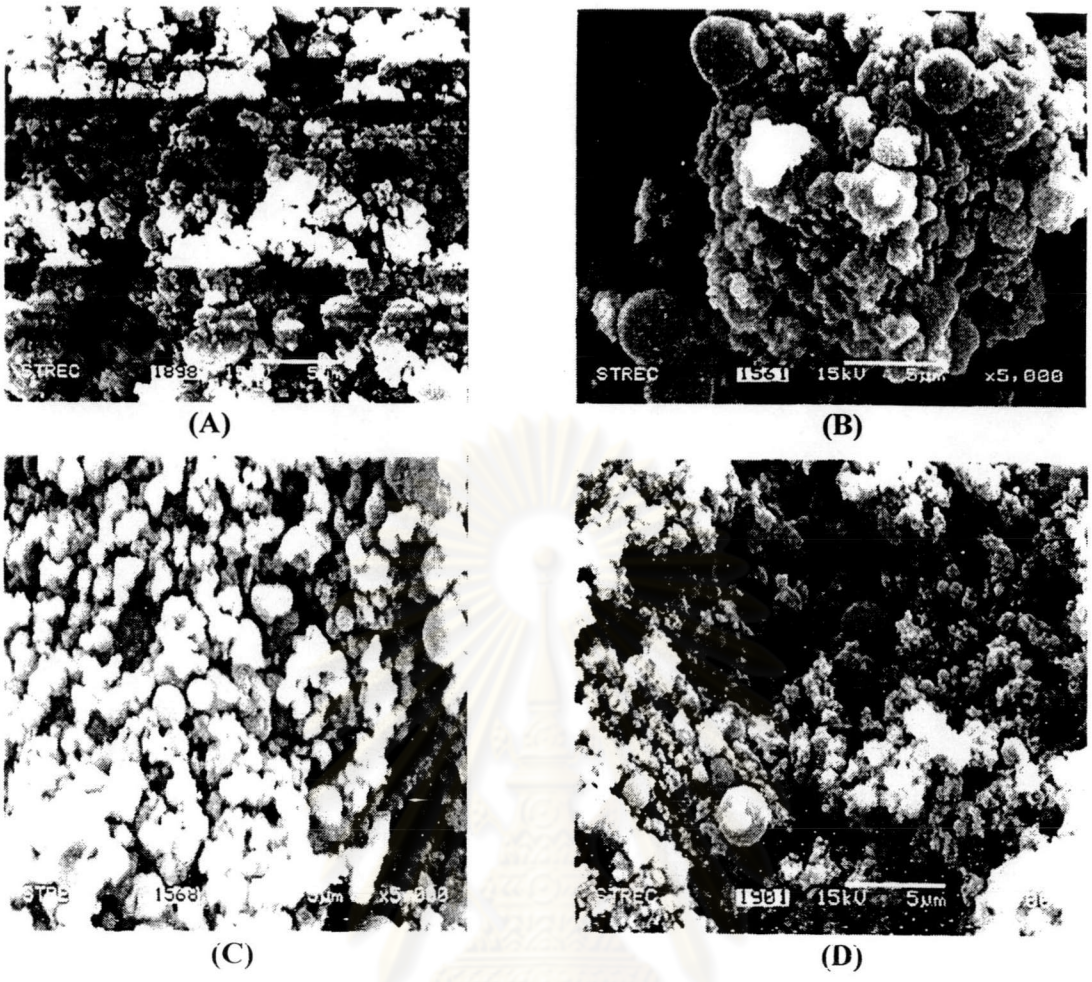


**Figure 5.6** SEM morphology of titania products synthesized in toluene for various reaction temperatures. (A) 270°C, (B) 300°C, (C) 320°C, and (D) 340°C.

### 5.1.2 Formation of iron (III) oxide and the effect of reaction temperature on iron (III) oxide product

The nanocrystallite iron (III) oxide synthesized in this work were prepared from iron acetylacetonate mixed with organic solvents; 1,4 butanediol or toluene at various reaction temperatures under autogeneous pressure.

#### 5.1.2.1 Reaction in 1,4-butanediol

Nanocrystalline iron (III) oxide was prepared in 1,4-butanediol at different reaction temperatures (220, 250, 300, 320 and 340°C) and hold at that temperature for 2 hours. The XRD patterns of the obtained product is given in Figure 5.7 indicated the formation of $\gamma$-$Fe_2O_3$ structure in all cases. No other crystalline phases were identified. At a temperature of 220°C, the sample showed strong diffraction peaks. The crystallite size calculated by the XRD broadening was 16.6 nm. The iron (III) oxide nanocrystals obtained at this temperature were smallest, while the broad peaks had a strong intensity. With increasing reaction temperature, the crystallite sized obtained increased from 16.6 nm at 220°C to 48.9 nm at 340°C. BET surface area of iron (III) oxide prepared at 220°C was 79.4 $m^2/g$. when the reaction temperature was increased, the BET surface area was gradually decreased. Table 5.3 shown the crystallite size and BET surface area of all product at various temperatures. For $S_1/S_2$, the values were more than the unity at the reaction temperature was 220°C. It will be proposed that the products contaminated with organic moiety. The values were decreased with increasing the reaction temperature.

The iron (III) oxide products were characterized by SEM for analyzing morphology of the products as shown in Figure 5.8. SEM pictures show the surface fracture of a sponge-like material with significant differences in reaction to the nanostructure SEM images of the product synthesized at 220°C shows an irregular and very rough surface that seems to indicate the presence of very large pore. On the contrary, with the higher reaction temperatures, SEM picture is characterized by a finer roughness surface, probable indicating that smaller pores have formed during the glycothermal process (Solinas et al., 2001).

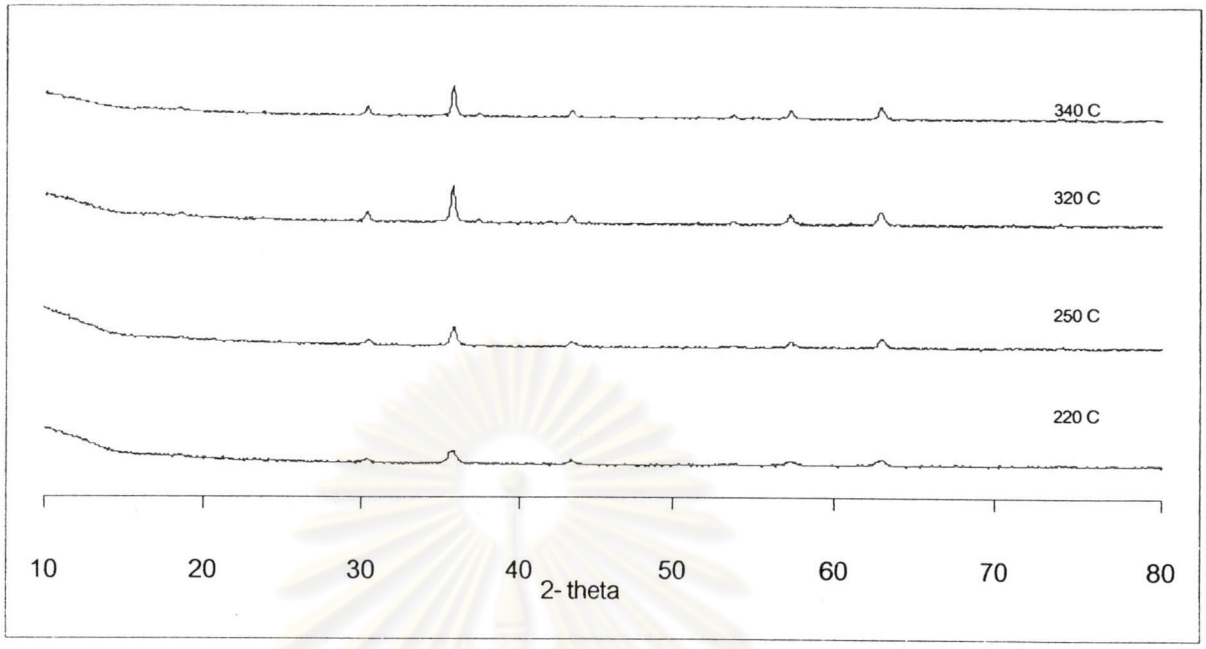


**Figure 5.7** XRD patterns of iron (III) oxide products synthesized in 1,4-BG for various reaction temperatures.

**Table 5.3** Crystallite size and surface area of iron (III) oxide products synthesized in 1,4-BG at different reaction temperatures.

| Reaction Temperature (°C) | Crystallite size (nm) | Surface area ($m^2/g$) | | $S_1/S_2$ |
|---|---|---|---|---|
| | | $S_1$[a] | $S_2$[b] | |
| 220 | 16.6 | 79.4 | 69.5 | 1.1 |
| 250 | 24.5 | 38.0 | 47.1 | 0.8 |
| 300 | 24.7 | 37.4 | 46.8 | 0.8 |
| 320 | 46.9 | 22.7 | 24.6 | 0.9 |
| 340 | 48.9 | 13.4 | 23.6 | 0.6 |

[a]Specific BET surface area from BET measurement

[b]Specific surface area calculated from equation of $6/d\rho$ on assumption that the crystal is nonporous spheres and using the density of anatase of 4.2 $g/cm^3$

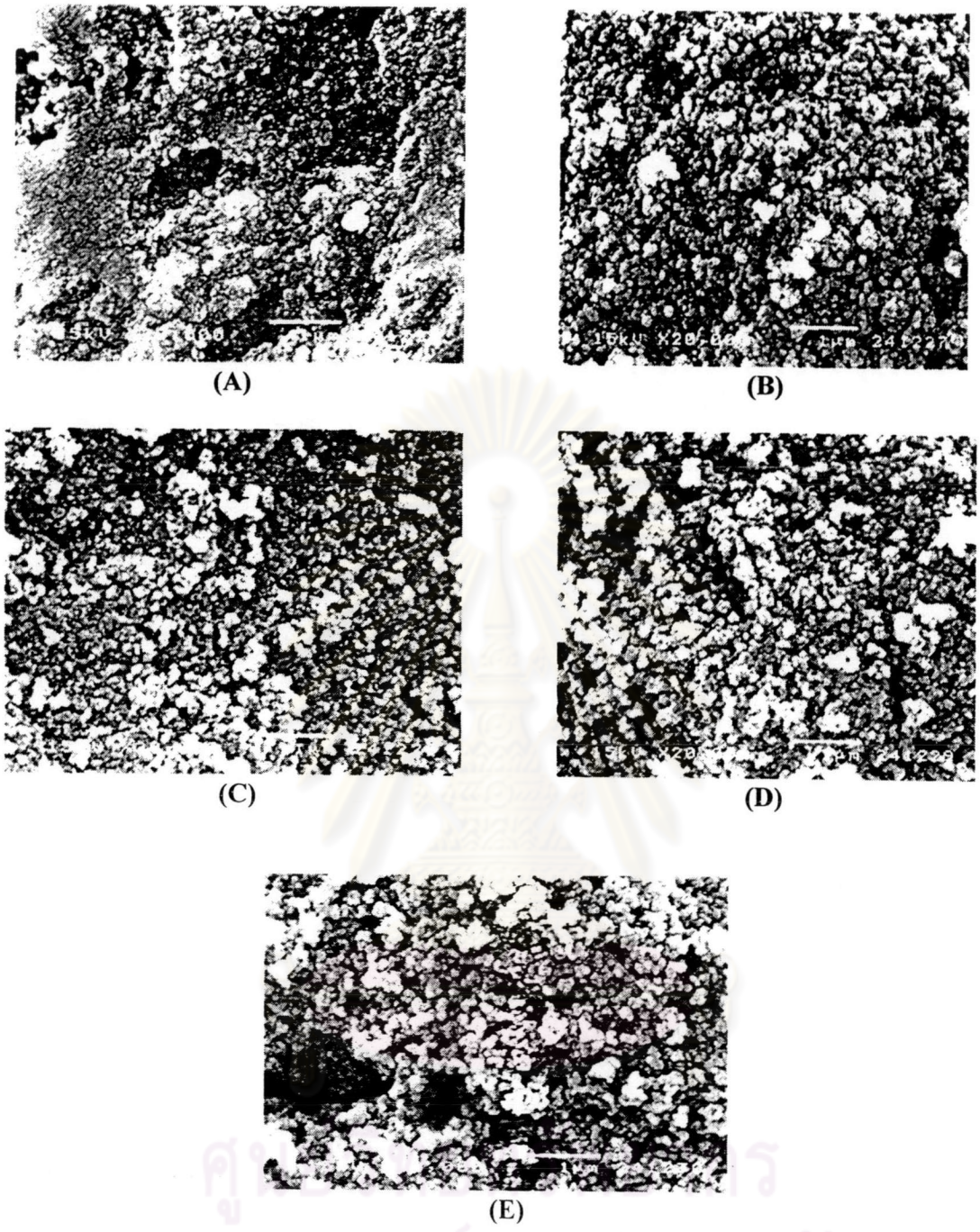


**Figure 5.8** SEM morphology of iron (III) oxide products synthesized in 1,4-BG for various reaction temperatures. (A) 220°C, (B) 250°C, (C) 300°C, (D) 320°C, and (E) 340°C.

### 5.1.2.2 Reaction in toluene

Iron (III) acetylacetonate was used to react with 100 ml of toluene at various reaction temperatures for 2 hours. These reaction temperatures were varied to 220, 250, 300, 320, and 340°C. The synthesized product at 220°C appeared amorphous phase, increasing the temperature of reaction to 250, 300, 320 and 340°C all of the as-synthesized iron (III) oxide yielded the maghemite iron (III) oxide ($\gamma$-$Fe_2O_3$). Evidence was obtained from XRD patterns of $\gamma$-$Fe_2O_3$ without the other phases as illustrated in Figure 5.9.

The crystallite size and the specific surface area are shown in Table 5.4. At a higher reaction temperature, the crystallite size was rather large (48.8 nm) under this reaction condition. The BET surface decreased with an increased of the reaction temperature. The $S_1/S_2$ values were more than the unity at the reaction temperature was 250 and 300°C and decreased to 0.8 when the reaction temperature increased to 340°C.

The relevant SEM micrographs of the products are shown in Figure 5.10. A lot of globular clusters along with acicular shape bars of $\gamma$-$Fe_2O_3$ are observed, indicating that the $\gamma$-$Fe_2O_3$ particles are agglomerated. When the synthesized temperature increase to 320°C, the surface of globular clusters becomes much rougher and the acicular shape bars become shorter evidently. (Jing and Wu., 2003).

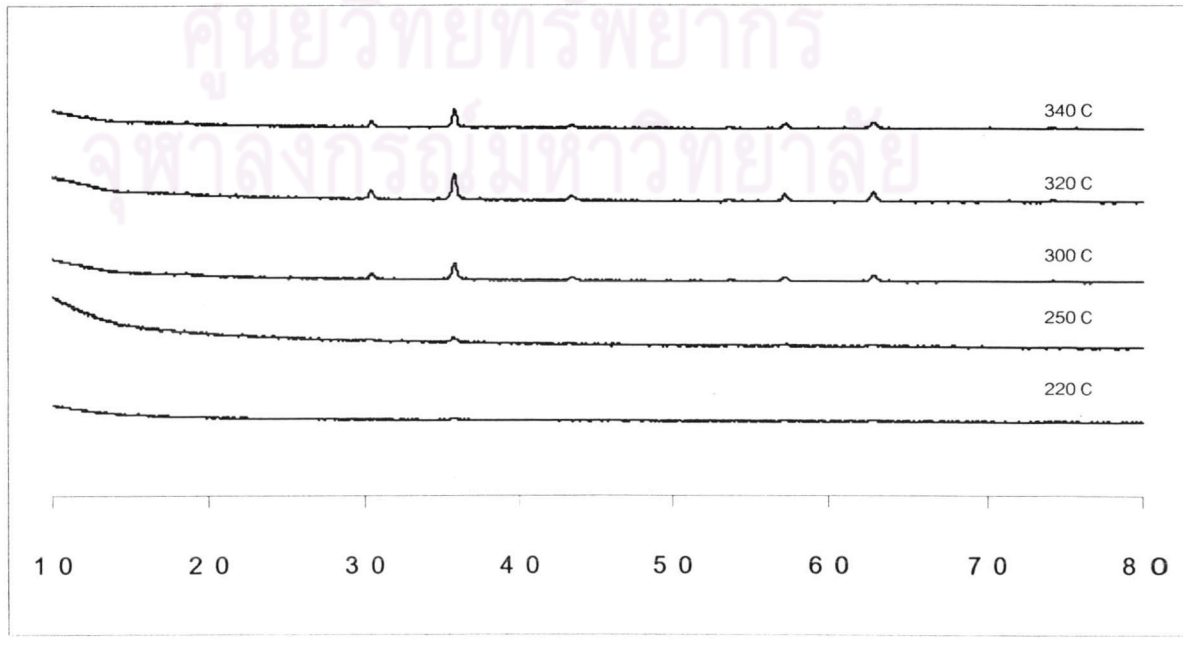


**Figure 5.9** XRD patterns of iron (III) oxide products synthesized in toluene for various

**Table 5.4** Crystallite size and surface area of iron (III) oxide products synthesized in toluene at different reaction temperature.

| Reaction Temperature (°C) | Crystallite size (nm) | Surface area ($m^2/g$) | | $S_1/S_2$ |
|---|---|---|---|---|
| | | $S_1$[a] | $S_2$[b] | |
| 220 | amorphous | - | - | - |
| 250 | 22.4 | 72.7 | 51.6 | 1.4 |
| 300 | 38.1 | 55.1 | 30.3 | 1.8 |
| 320 | 42.6 | 20.4 | 27.1 | 0.8 |
| 340 | 48.8 | 18.0 | 23.6 | 0.8 |

[a]Specific BET surface area from BET measurement

[b]Specific surface area calculated from equation of $6/d\rho$ on assumption that the crystal is nonporous spheres and using the density of anatase of 4.2 $g/cm^3$

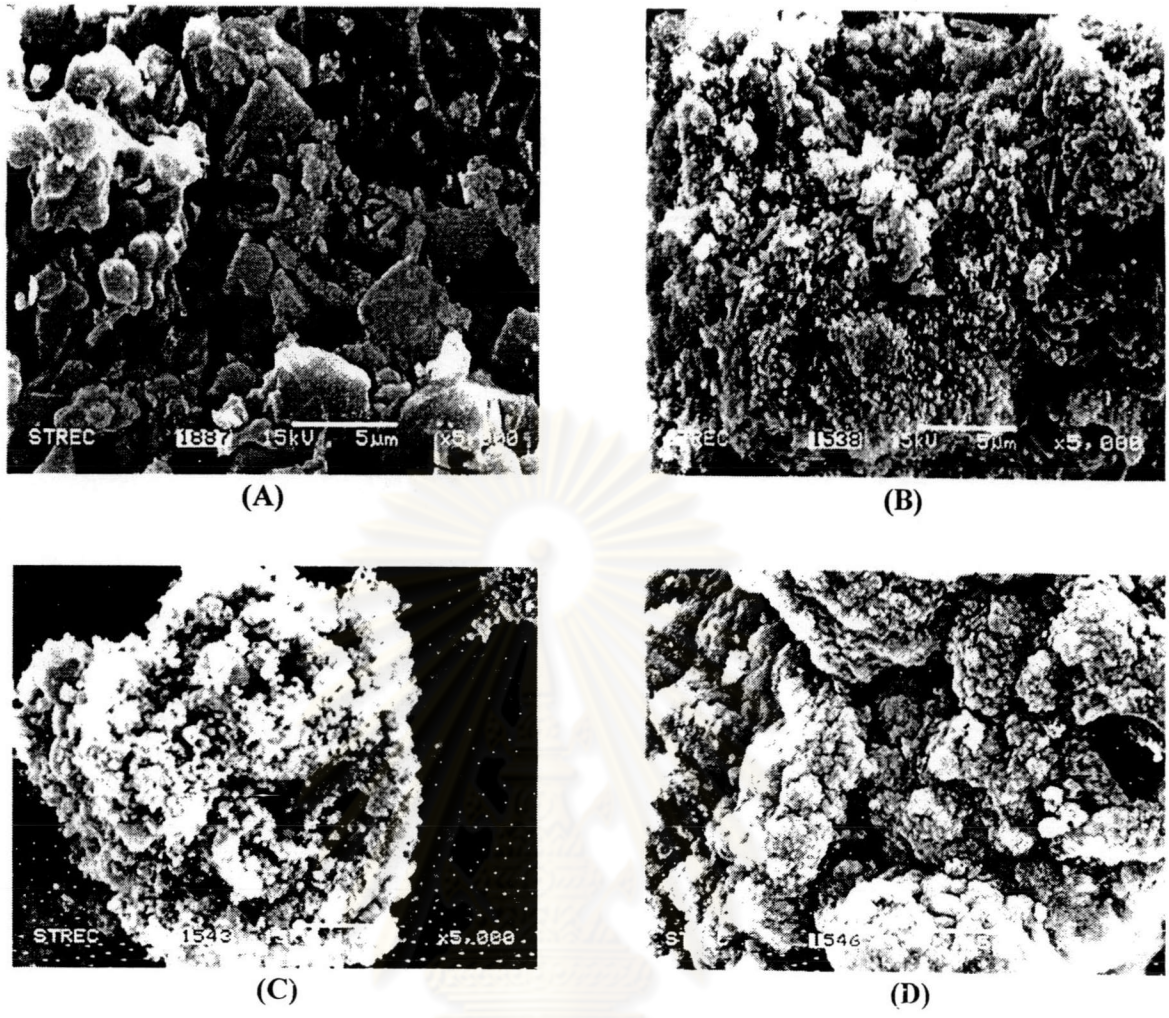


**Figure 5.10** SEM morphology of iron (III) oxide products synthesized in toluene for various temperatures. (A) 250°C, (B) 300°C, (C) 320°C, and (D) 340°C.

### 5.1.3 Formation of zinc (II) oxide and the effect of reaction temperature on zinc (II) oxide product

The reaction of zinc (II) acetylacetonate with organic solvents, 1,4-butanediol or toluene were done in this work. The synthesized temperatures were varied under autogeneous pressure.

#### 5.1.3.1 Reaction in 1,4-butanediol

Zinc (II) oxide was synthesized for various reaction temperature (200, 220, 250, 270, 300 and 320°C). The typical XRD patterns for the crystalline zinc (II) oxide powders obtained in different reaction temperatures are shown in Figure 5.11. The sharp diffraction peaks of the powder imply their good crystallinity. All diffraction peaks in the XRD patterns of as-prepared ZnO can be assigned to the hexagonal structure, which indicates that phase-pure hexagonal structure ZnO has been successfully synthesized in various reaction temperatures via this glycothermal method. Specific surface area and the crystallite size are summarized in Table 5.5 indicated that the crystallite size of zinc oxide obtained in this reaction are significantly varied with the reaction temperature which is 14.3 nm at 200°C and increases to 92.5 at 320°C. In contrast, the specific surface areas obtained from both BET measurement and calculation was decreased with increasing the reaction temperature.

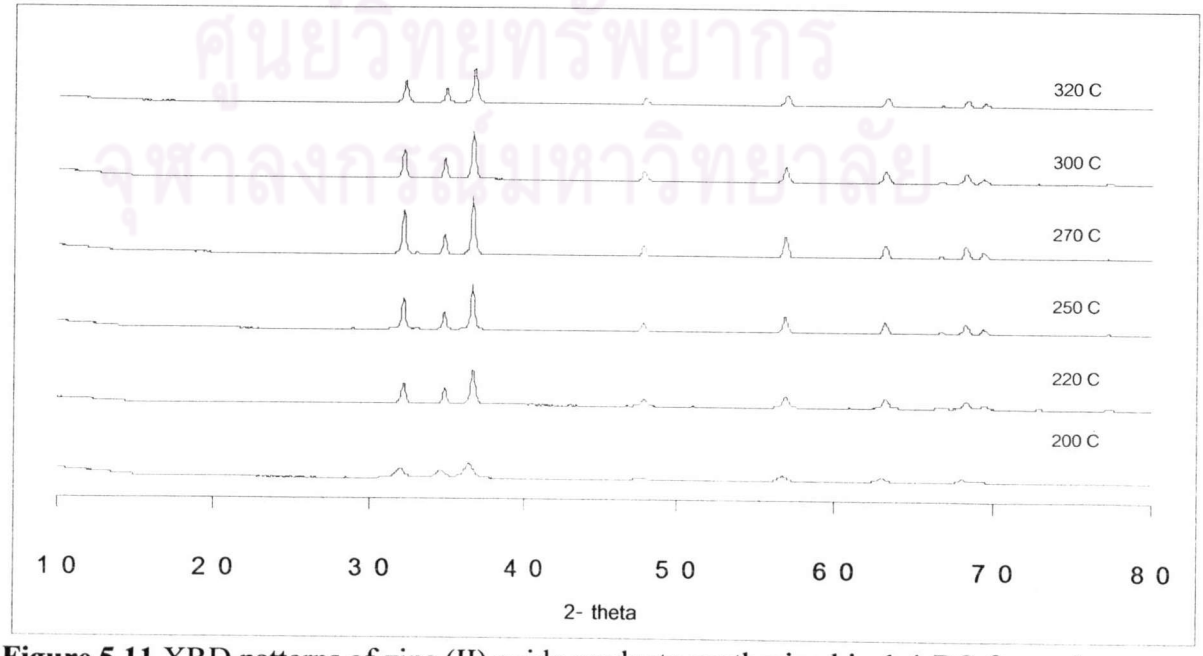


**Figure 5.11** XRD patterns of zinc (II) oxide products synthesized in 1,4-BG for various reaction temperatures.

**Table 5.5** Crystallite size and surface area of zinc (II) oxide products synthesized in 1,4-BG at different reaction temperature.

| Reaction Temperature (°C) | Crystallite size (nm) | Surface area ($m^2/g$) | | $S_1/S_2$ |
|---|---|---|---|---|
| | | $S_1$[a] | $S_2$[b] | |
| 200 | 14.3 | 39.0 | 74.7 | 0.5 |
| 220 | 39.2 | 20.6 | 27.3 | 0.8 |
| 250 | 53.9 | 17.8 | 19.9 | 0.9 |
| 270 | 67.6 | 13.2 | 15.8 | 0.8 |
| 300 | 68.9 | 12.1 | 15.6 | 0.8 |
| 320 | 92.5 | 12.0 | 11.6 | 1.0 |

[a]Specific BET surface area from BET measurement

[b]Specific surface area calculated from equation of $6/d\rho$ on assumption that the crystal is nonporous spheres and using the density of anatase of 4.2 $g/cm^3$

For $S_1/S_2$ value, it was gradually increased with increasing the reaction temperature. These indicated that the crystal was formed to free-flow crystal.

The SEM image of the ZnO powders prepared by glycothermal treatment of zinc (II) acetylacetonate and 1,4-BG for various reaction temperature are shown in Figure 5.12. It is observed that the morphology of the obtained ZnO particles changes in turn from lumpy surface to rod-like when increasing the reaction temperature (Chen et al., 2000).

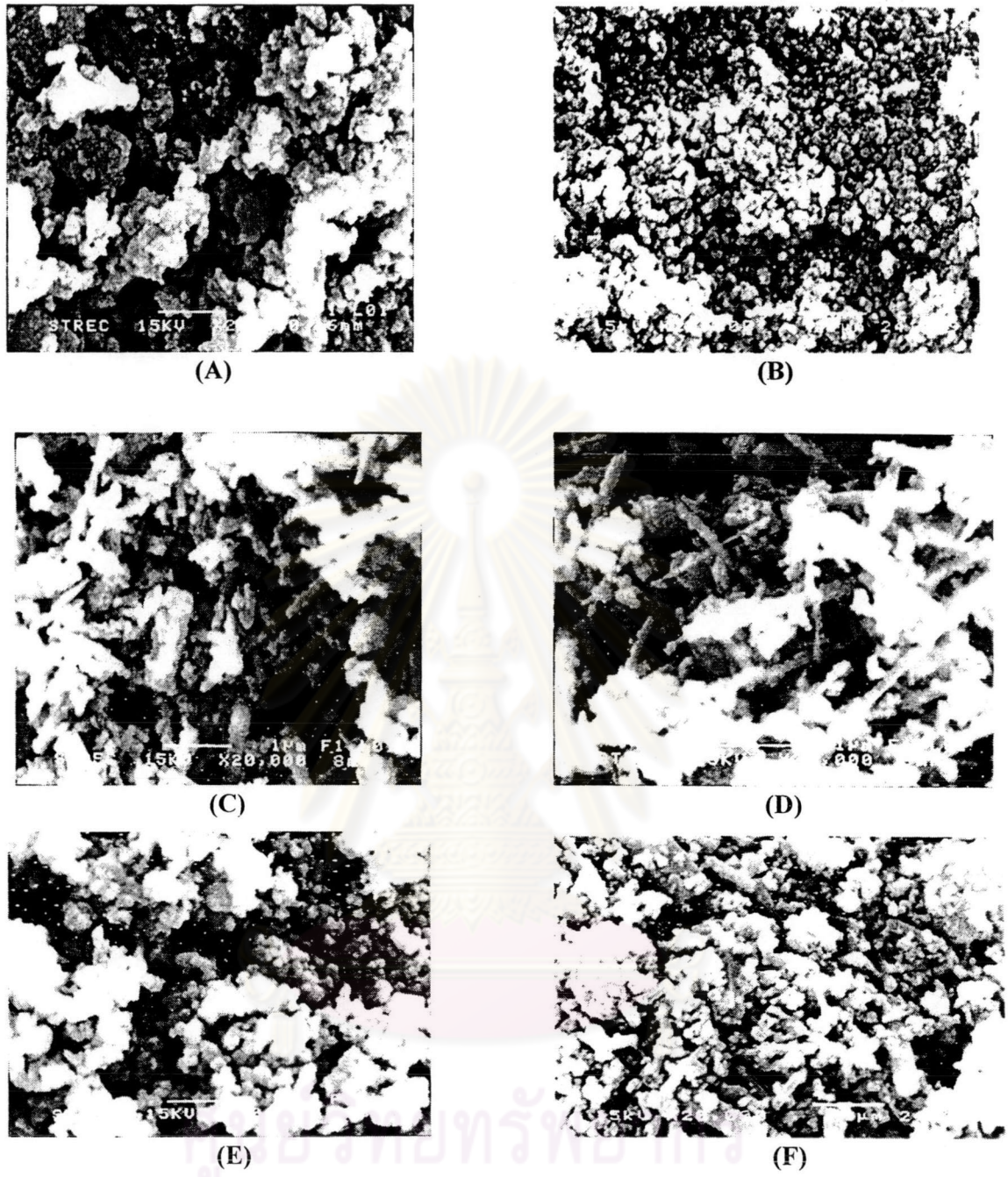


**Figure 5.12** SEM morphology of zinc (II) oxide products synthesized in 1,4-BG for various reaction temperatures. (A) 200°C, (B) 220°C, (C) 250°C, (D) 270°C, (E) 300°C, and (F) 320°C.

### 5.1.3.2 Reaction in toluene

Crystallite zinc oxide powders have been prepared by solvothermal treatment of zinc (II) acetylacetonate in toluene under autogeneous pressure for 2 hours at various reaction temperature (200, 220, 250, 270, 300, and 320°C). The XRD patterns of obtained powders are shown in Figure 5.13. It is found that all specimens become zinc oxide powder with well-developed crystallinity. It reveals that zinc oxide powder was directly synthesized during the solvothermal process. All diffraction peaks are assigned to ZnO, indicating that the produced powder was monophasic zincite with a hexagonal structure.

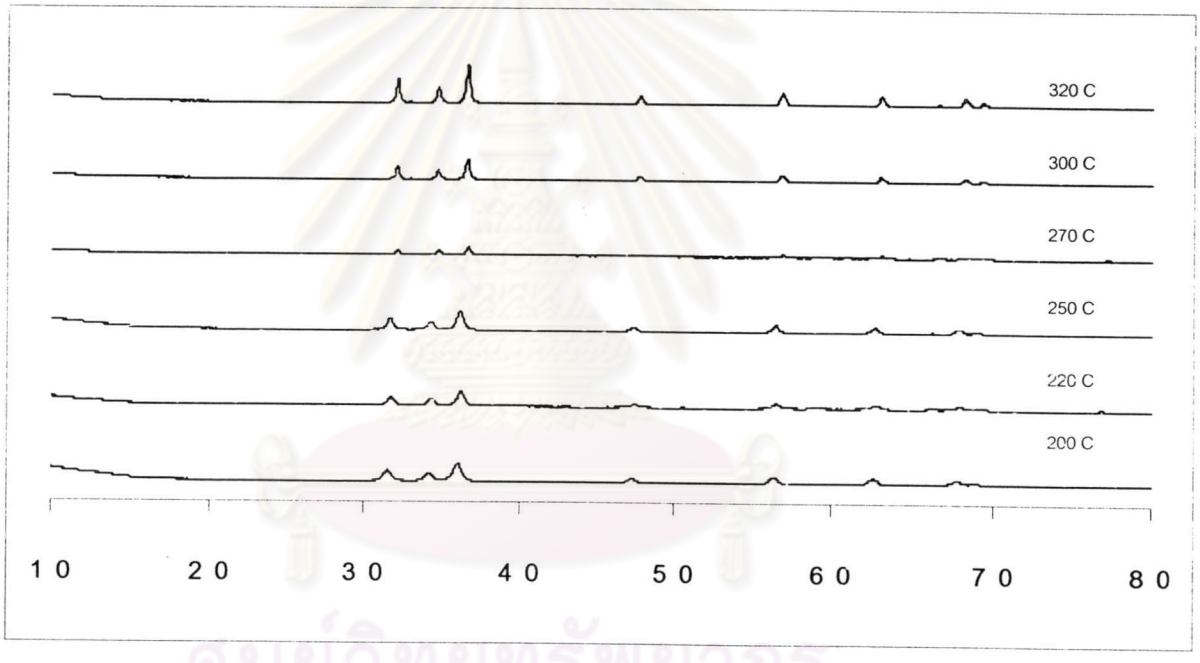


**Figure 5.13** XRD patterns of zinc (II) oxide products synthesized in toluene for various reaction temperatures.

Table 5.6 presents the crystallite size and the specific surface area of zinc (II) oxide which shows that at 200°C the crystallite size of ZnO powder is around 16.4 nm; however, it is raised to 54.5 nm, when the reaction temperature increased to 320°C. On the other hand the specific surface area decreases with an increase of the reaction temperature.

The nanostructure of ZnO powder prepared at different heating temperature are shown in Figure 5.14. It is observed that at the reaction temperature was 200-270°C, the particles exhibited lumpy surface and observed the small particles with a rod-like treated at high reaction temperature.

**Table 5.6** Crystallite size and surface area of zinc (II) oxide products synthesized in toluene at different reaction temperatures.

| Reaction Temperature (°C) | Crystallite size (nm) | Surface area ($m^2/g$) | | $S_1/S_2$ |
|---|---|---|---|---|
| | | $S_1$[a] | $S_2$[b] | |
| 200 | 16.4 | 37.3 | 65.3 | 0.6 |
| 220 | 18.7 | 26.2 | 57.3 | 0.5 |
| 250 | 24.8 | 24.7 | 43.2 | 0.6 |
| 270 | 39.5 | 14.2 | 27.1 | 0.5 |
| 300 | 35.4 | 12.6 | 30.2 | 0.4 |
| 320 | 54.5 | 8.8 | 19.7 | 0.5 |

[a]Specific BET surface area from BET measurement

[b]Specific surface area calculated from equation of $6/d\rho$ on assumption that the crystal is nonporous spheres and using the density of anatase of 4.2 $g/cm^3$

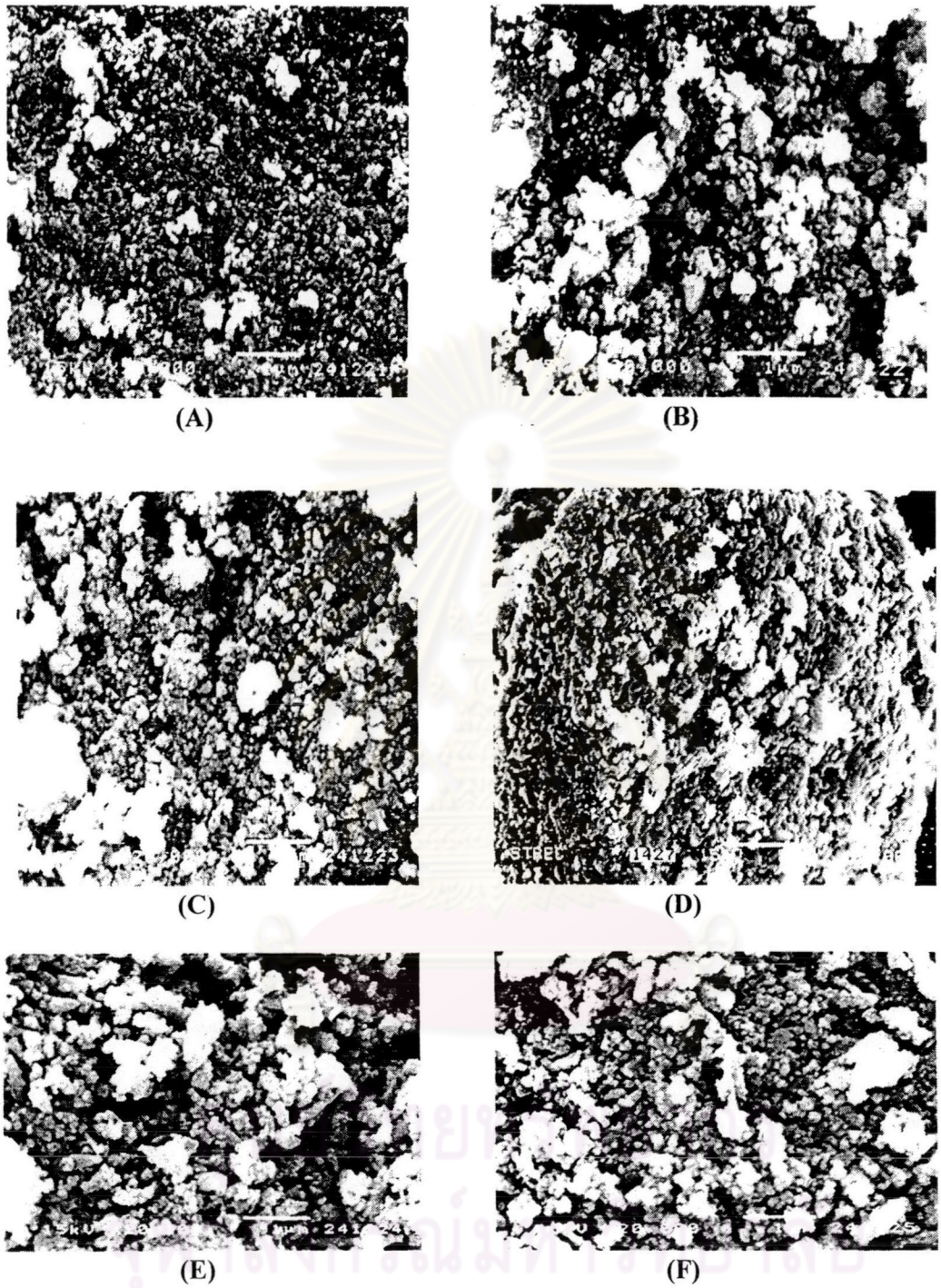

**Figure 5.14** SEM morphology of zinc (II) oxide products synthesized in toluene for various reaction temperatures. (A) 200°C, (B) 220°C, (C) 250°C, (D) 270°C, (E) 300°C, and (F) 320°C.

## 5.2 Effect of solvent and reaction temperature on the crystallite size of metal oxide product

### 5.2.1 Effect of solvent and reaction temperature on titanium (IV) oxide

Reaction of titanium tert-butoxide in 1,4-butanediol and toluene at various reaction temperatures for 2 hours under autogeneous pressure show that the increase in reaction temperature resulted in the increase in as-synthesized crystal. The as-synthesized crystallite size depend on the reaction temperature, which synthesized in both solvents.

Considering for the effects of solvent on the crystallite size, as seen from Figure 5.15. The synthesis in both 1,4-butanediol and toluene resulted in the nearly as-synthesized crystal size, which considered from the similar slope of the graph. For titanium (IV) oxide the different solvent are not affected the crystallite size.

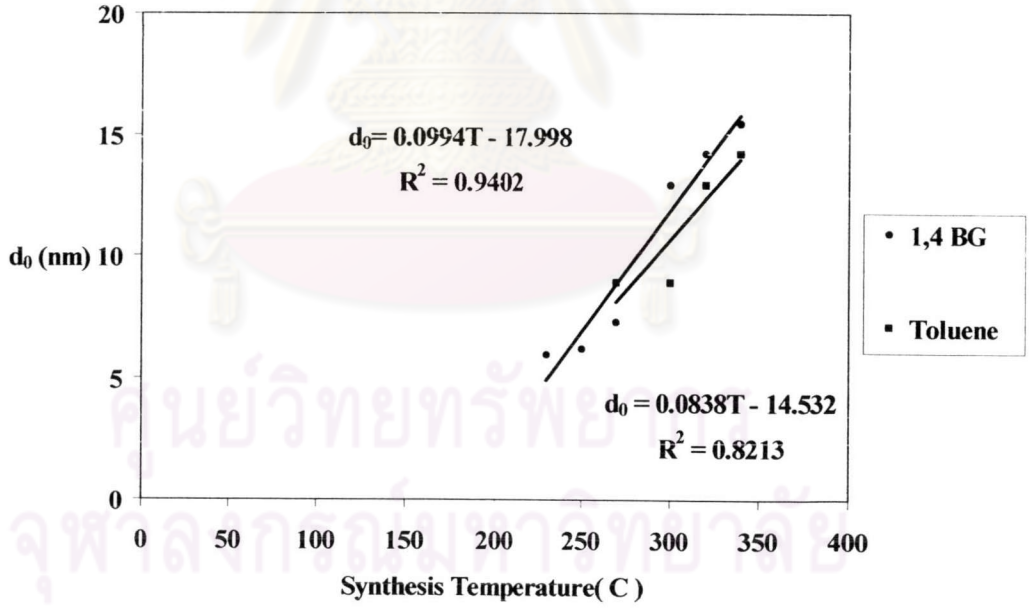


**Figure 5.15** Relation between reaction temperatures and solvents on the crystallite size of titanium (IV) oxide.

### 5.2.2 Effects of solvent and reaction temperature on iron (III) oxide

Nanocrystalline iron (III) oxide was prepared in 1,4-butanediol and toluene at different reaction temperatures. The crystallite size obtained at lower temperature was small, with increasing reaction temperature, the crystallite sized obtained increased. The relation between reaction temperature and solvent on the as-synthesized crystallite size of iron (III) oxide is shown in Figure 5.16.

The synthesis in both 1,4-butanediol and toluene exhibited in the similar as-synthesized crystal size. It was shown in the nearly slope that is 0.2618 and 0.2917. It was shown that both solvents resulted in the same crystallite size.

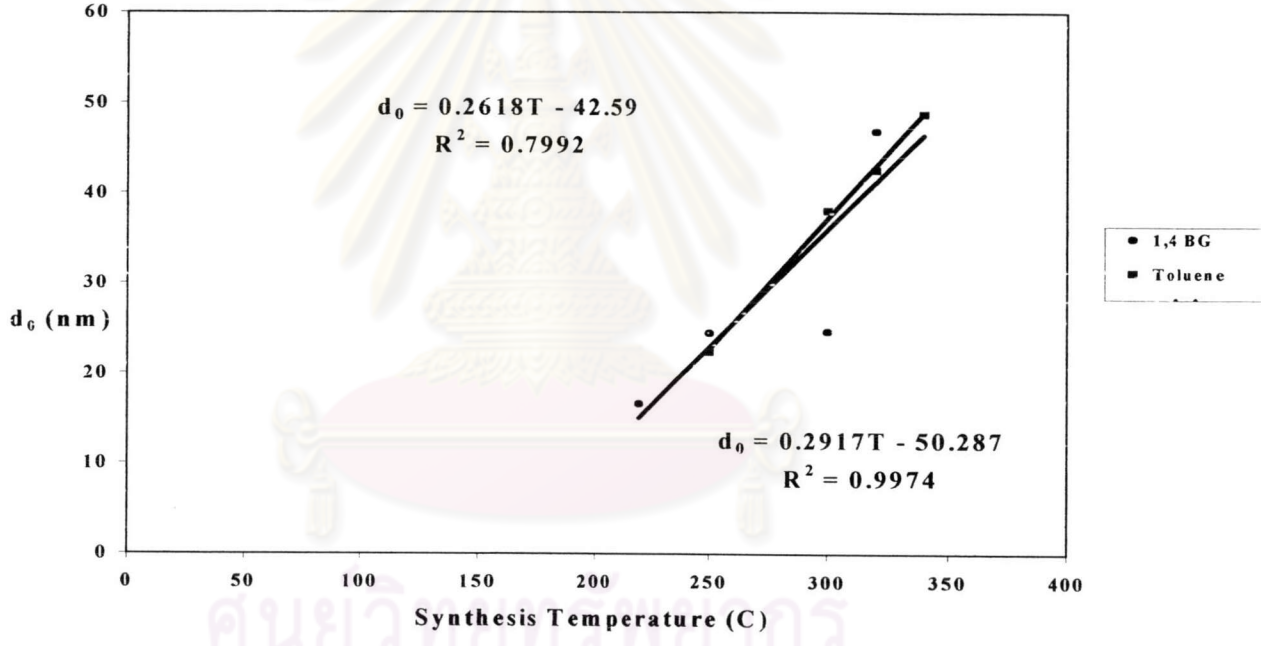


**Figure 5.16** Relation between reaction temperatures and solvents on the crystallite size of iron (III) oxide.

### 5.2.3 Effects of solvent and reaction temperature on zinc (II) oxide

Zinc (II) oxide was synthesized in 1,4-butanediol and toluene for various reaction temperatures. The results showed that the increase in reaction temperature resulted in the increase in as-synthesized crystallite size. The crystallite size of zinc (II) oxide obtained are significantly varied with the reaction temperature.

The growth of the as-synthesized crystal in two solvents are not the same as seen in Figure 5.17 that the growth of as-synthesized crystallite size in 1,4-butanediol are higher than the growth of crystal synthesized in toluene compared with different slope of both solvents. The growth after nucleation can be affected by the kind of solvents, because the particle interaction potential is different in each solvent. For zinc (II) oxide the different solvents are affected the crystallite size.

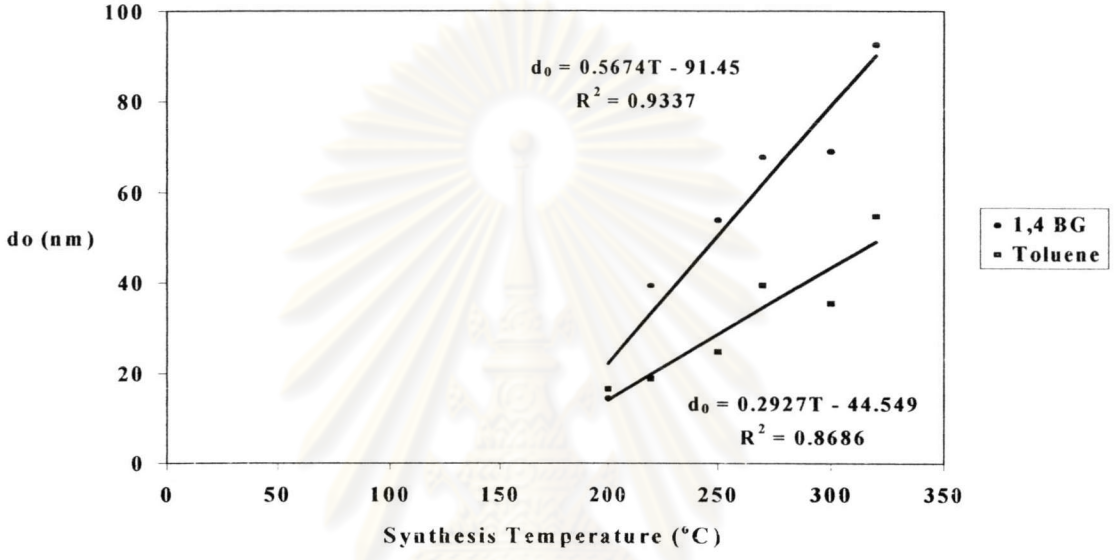


**Figure 5.17** Relation between reaction temperatures and solvents on the crystallite size of zinc (II) oxide.

## 5.3 Formation of silicon modified metal oxide

### 5.3.1 Formation of silicon modified titanium (IV) oxide

Reaction of titanium (IV) tert-butoxide and tetraethyl orthosilicate with the molar ratio Si/Ti of 0, 0.005, and 0.08 in 1,4-butanediol for various reaction temperatures (230, 250, 320, and 340°C). The XRD patterns of the products obtained with addition of TEOS revealed that all the products had the anatase structure and the peak intensities were not affected by the TEOS content in the reaction mixture as seen in Figure 5.18 to 5.21. The crystallite size of the as-synthesized silicon modified-titania and the product after calcination at 900°C are summarized in Table 5.7. With the increase of the amounts of TEOS added, the crystallite size decreased.

SEM images of the as-synthesized silicon modified-titania and the product after calcination at 900°C for 1 hour are presented in Figure 5.22 to 5.25. As seen from SEM pictures for all reaction temperatures the morphology of silicon modified titania did not changed with increasing the amount of silicon. The shape of the secondary particle was an irregular particle.

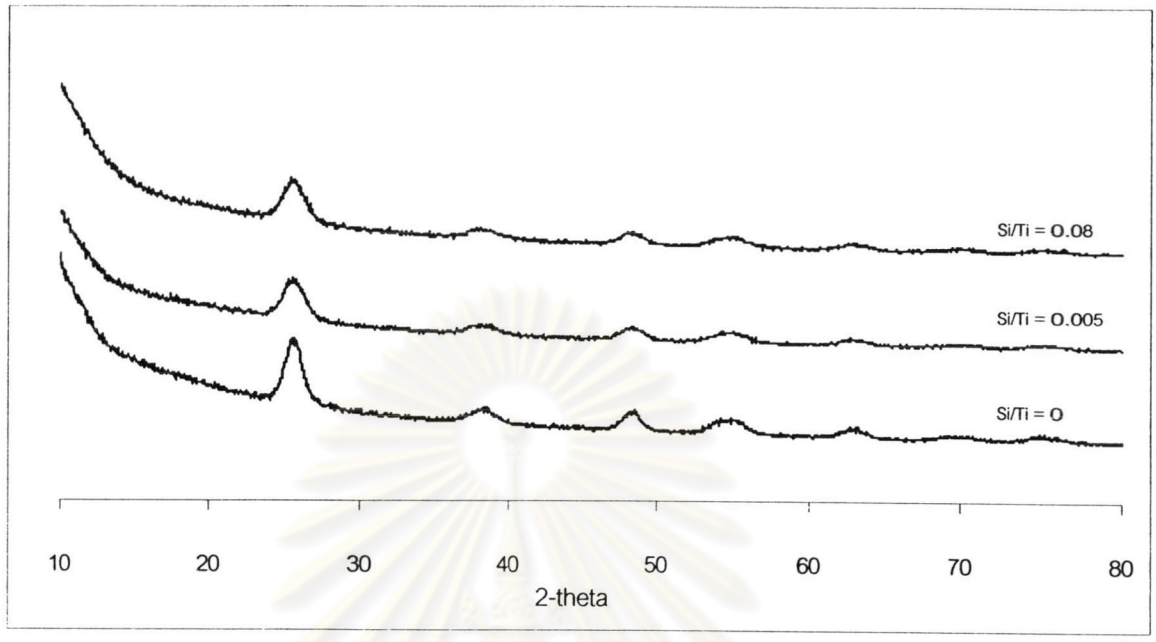


**Figure 5.18** XRD patterns of silicon modified titania products for various silicon contents at 230°C.

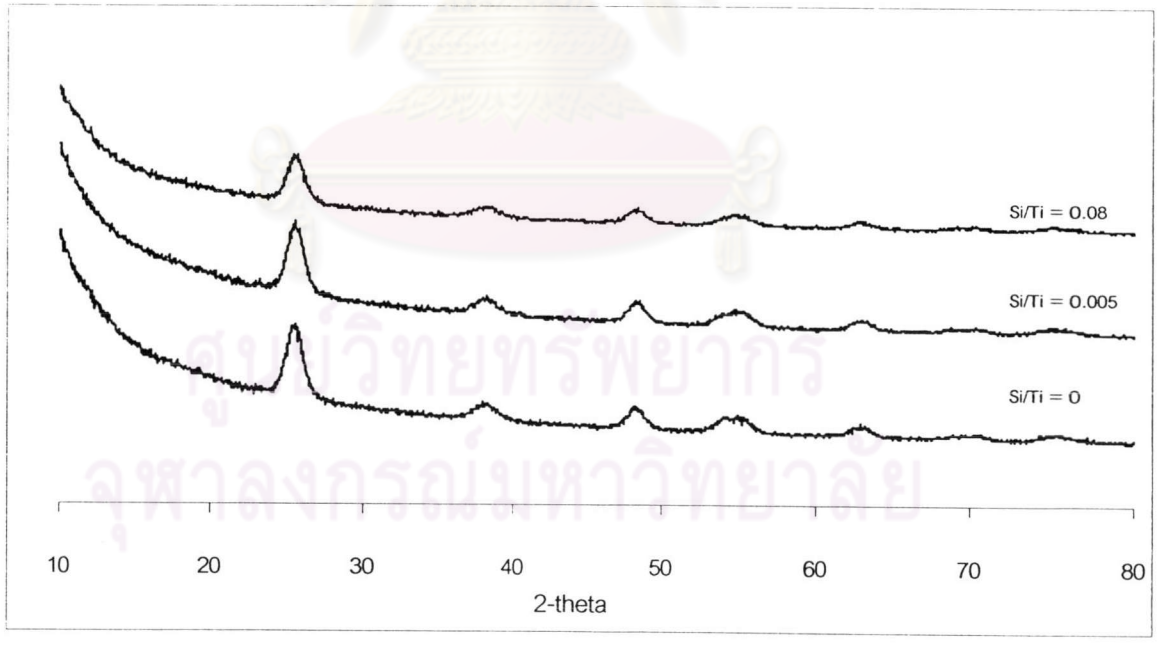


**Figure 5.19** XRD patterns of silicon modified titania products for various silicon contents at 250°C.

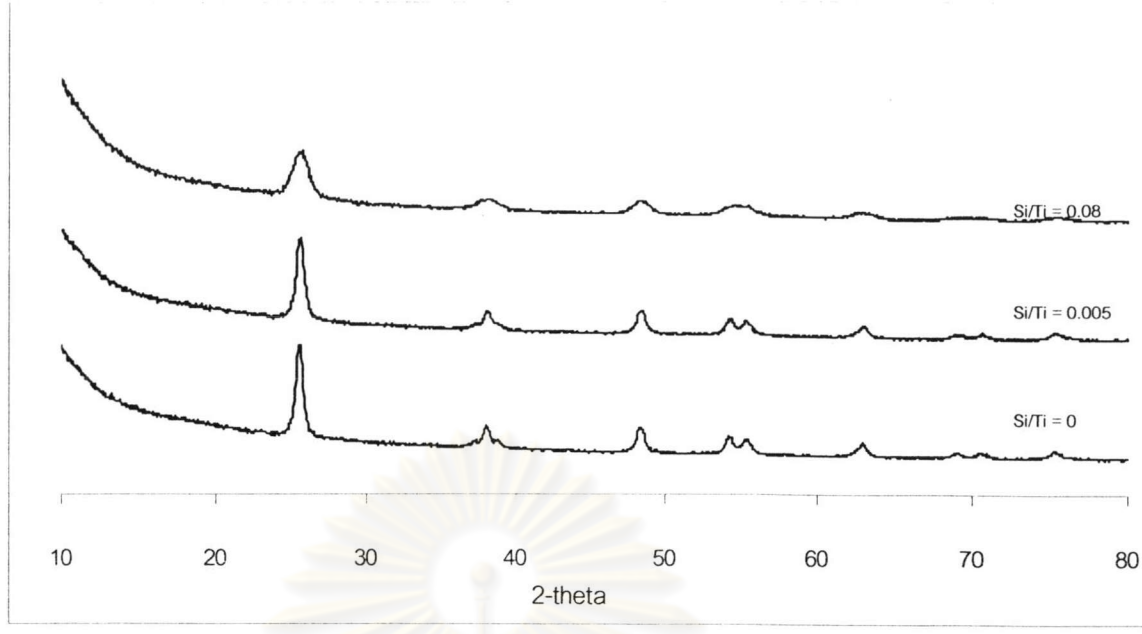


**Figure 5.20** XRD patterns of silicon modified titania products for various silicon contents at 320°C

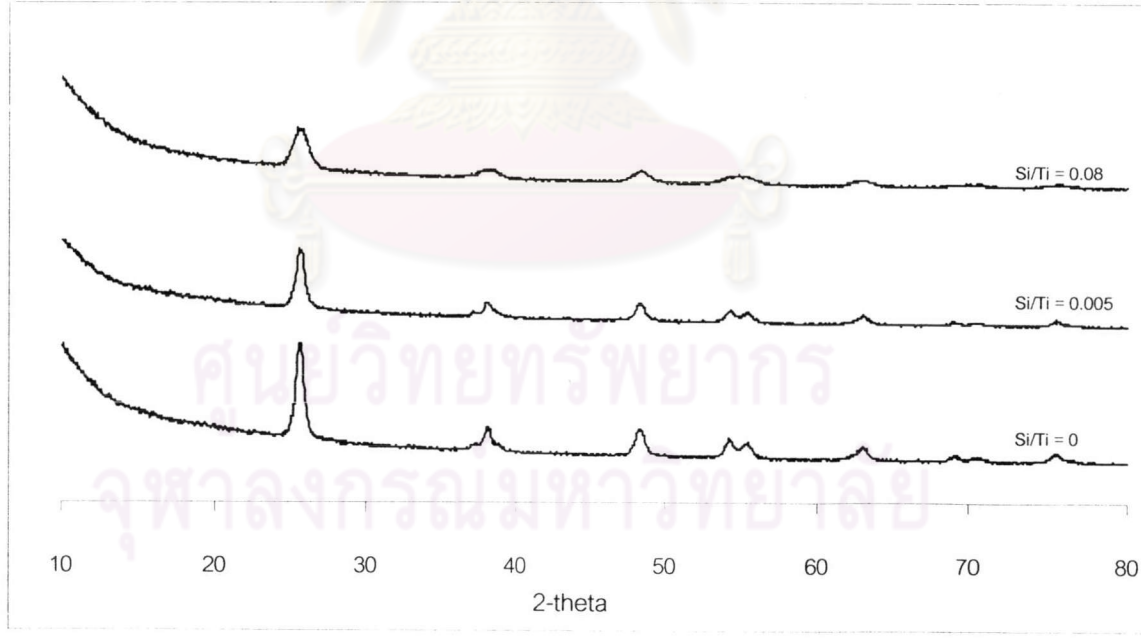


**Figure 5.21** XRD patterns of silicon modified titania products for various silicon contents at 340°C

**Table 5.7** Crystallite size data of titanium (IV) oxide synthesized at various reaction temperature for the different molar ratio of Si/Ti before calcination ($d_0$) and calcined product of 900°C ($d_{900}$)

| Reaction Temperature (°C) | Charged Si/Ti ratio | Crystallite size (nm) | | $d_{900}/d_0$ |
|---|---|---|---|---|
| | | $d_0$ | $d_{900}$ | |
| 230 | 0 | 5.9 | 35.0 | 5.9 |
| | 0.005 | 4.7 | 19.6 | 4.2 |
| | 0.08 | 4.6 | 20.0 | 4.3 |
| 250 | 0 | 6.2 | 37.0 | 6.0 |
| | 0.005 | 6.5 | 39.6 | 6.1 |
| | 0.08 | 6.5 | 15.4 | 2.4 |
| 320 | 0 | 14.2 | 44.0 | 3.1 |
| | 0.005 | 12.9 | 32.3 | 2.5 |
| | 0.08 | 7.1 | 17.9 | 2.5 |
| 340 | 0 | 15.4 | 36.7 | 2.4 |
| | 0.005 | 14.2 | 30.6 | 2.2 |
| | 0.08 | 6.5 | 19.9 | 3.1 |

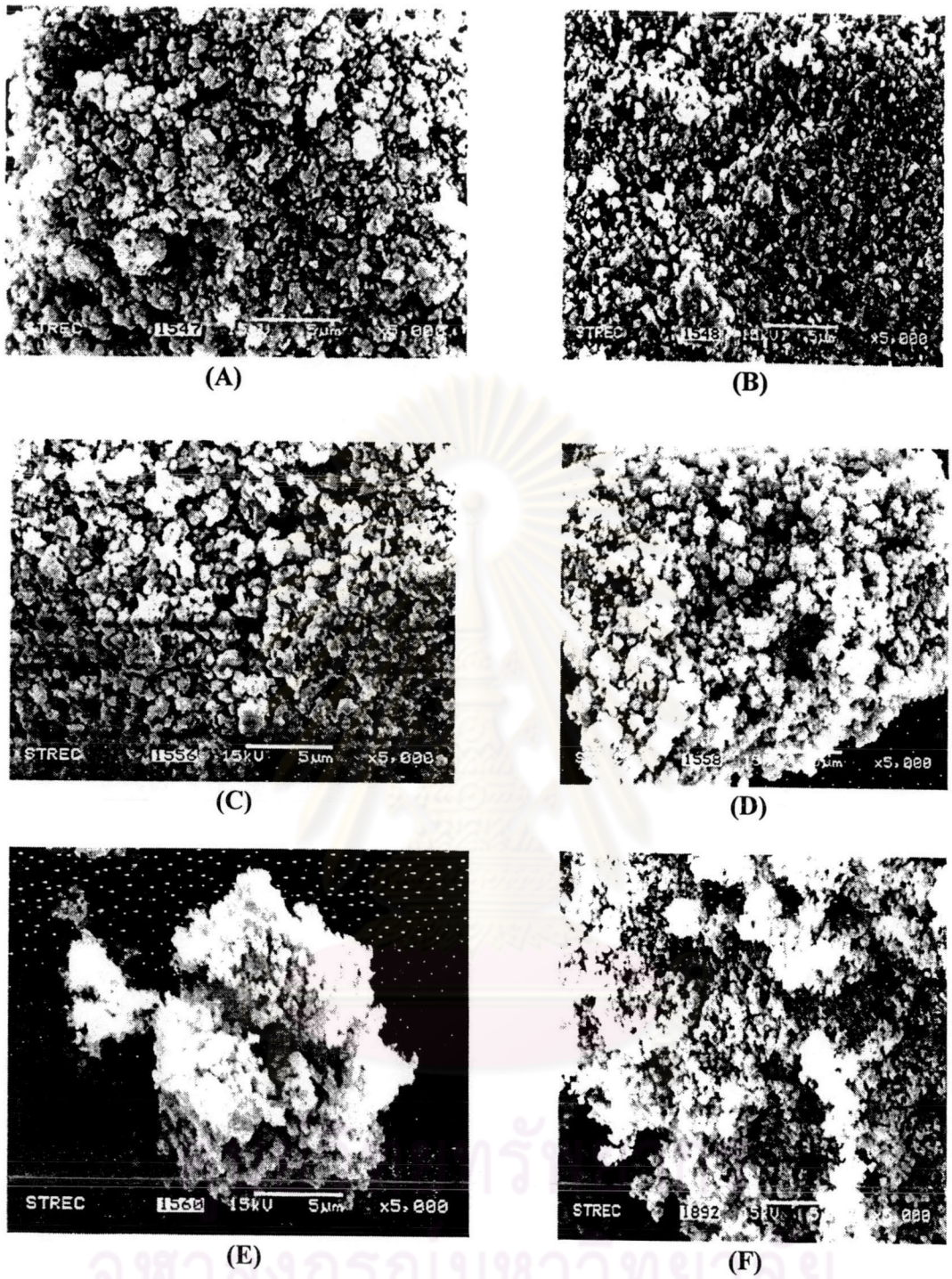


**Figure 5.22** SEM morphology of silicon modified titania products at 230°C. (A) Pure titania, as-synthesized, (B) Pure titania, calcined 900°C, (C) Si/Ti 0.005, as-synthesized, (D) Si/Ti 0.005, calcined 900°C, (E) Si/Ti 0.08, as-synthesized, and (F) Si/Ti 0.08 calcined 900°C.

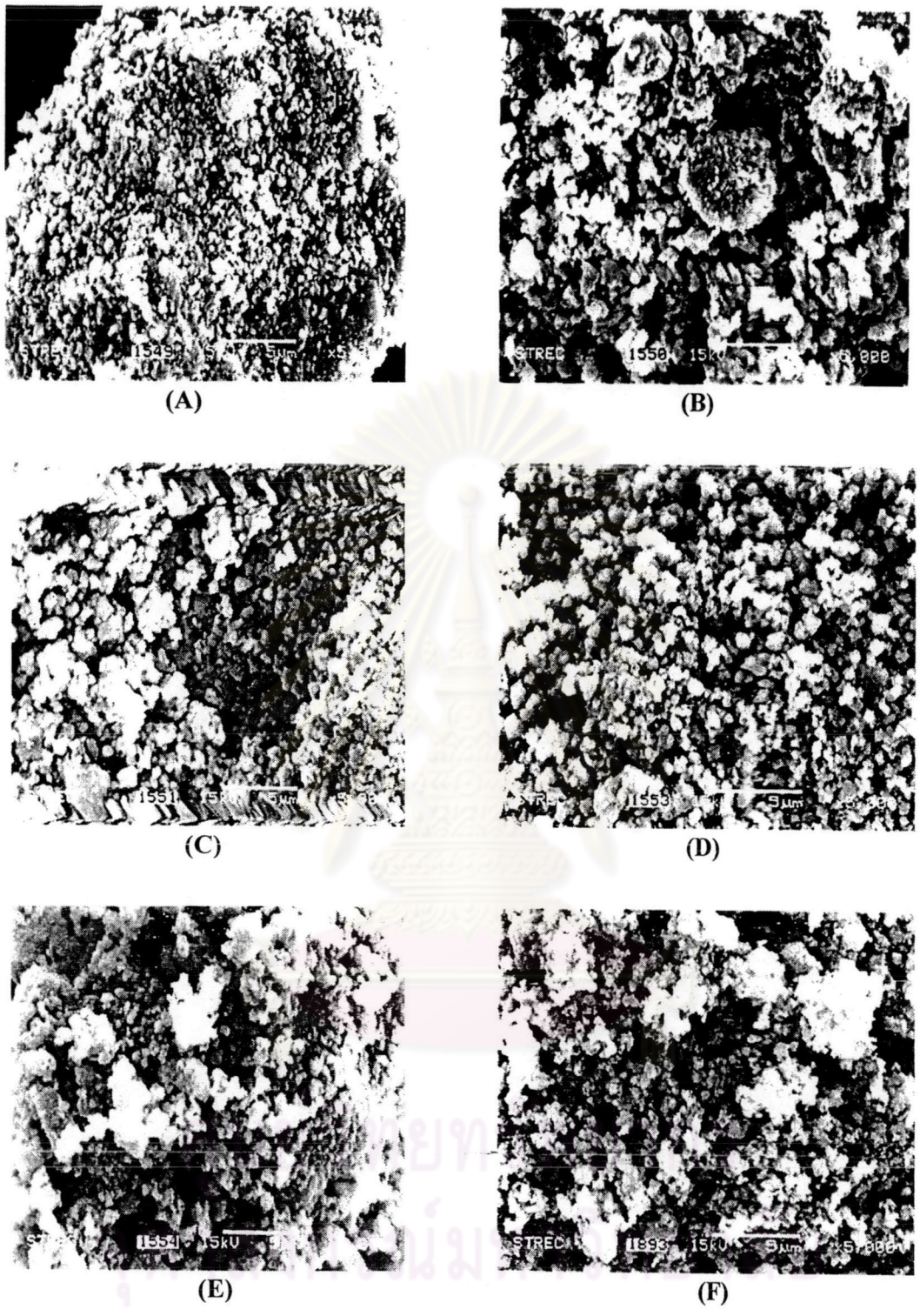

**Figure 5.23** SEM morphology of silicon modified titania products at 250°C.
(A) Pure titania, as-synthesized, (B) Pure titania, calcined 900°C, (C) Si/Ti 0.005, as-synthesized, (D) Si/Ti 0.005, calcined 900°C, (E) Si/Ti 0.08, as-synthesized, and (F) Si/Ti 0.08, calcined 900°C.

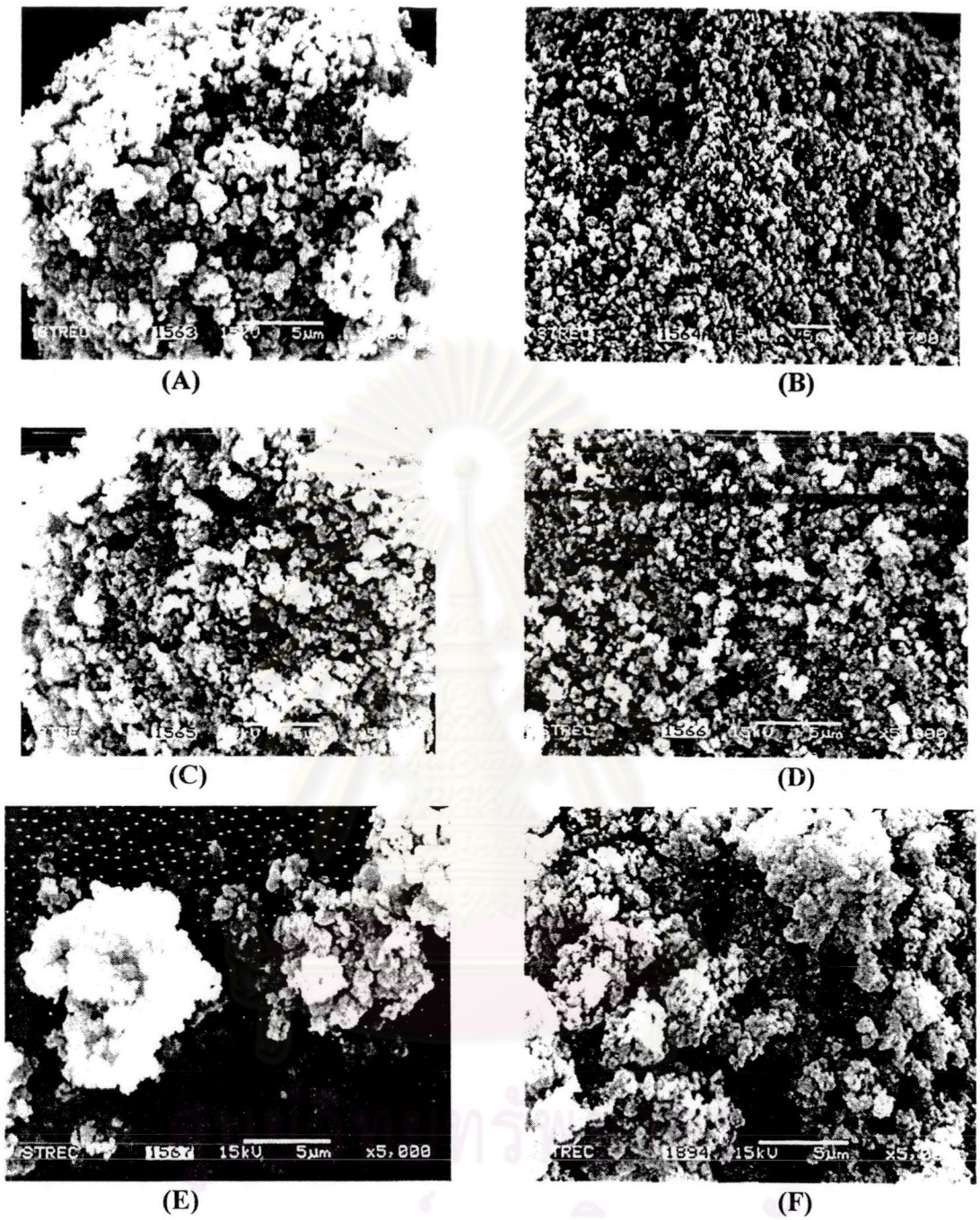


**Figure 5.24** SEM morphology of silicon modified titania products at 320°C. (A) Pure titania, as-synthesized, (B) Pure titania, calcined 900°C, (C) Si/Ti 0.005, as-synthesized, (D) Si/Ti 0.005, calcined 900°C, (E) Si/Ti 0.08, as-synthesized, and (F) Si/Ti 0.08, calcined 900°C.

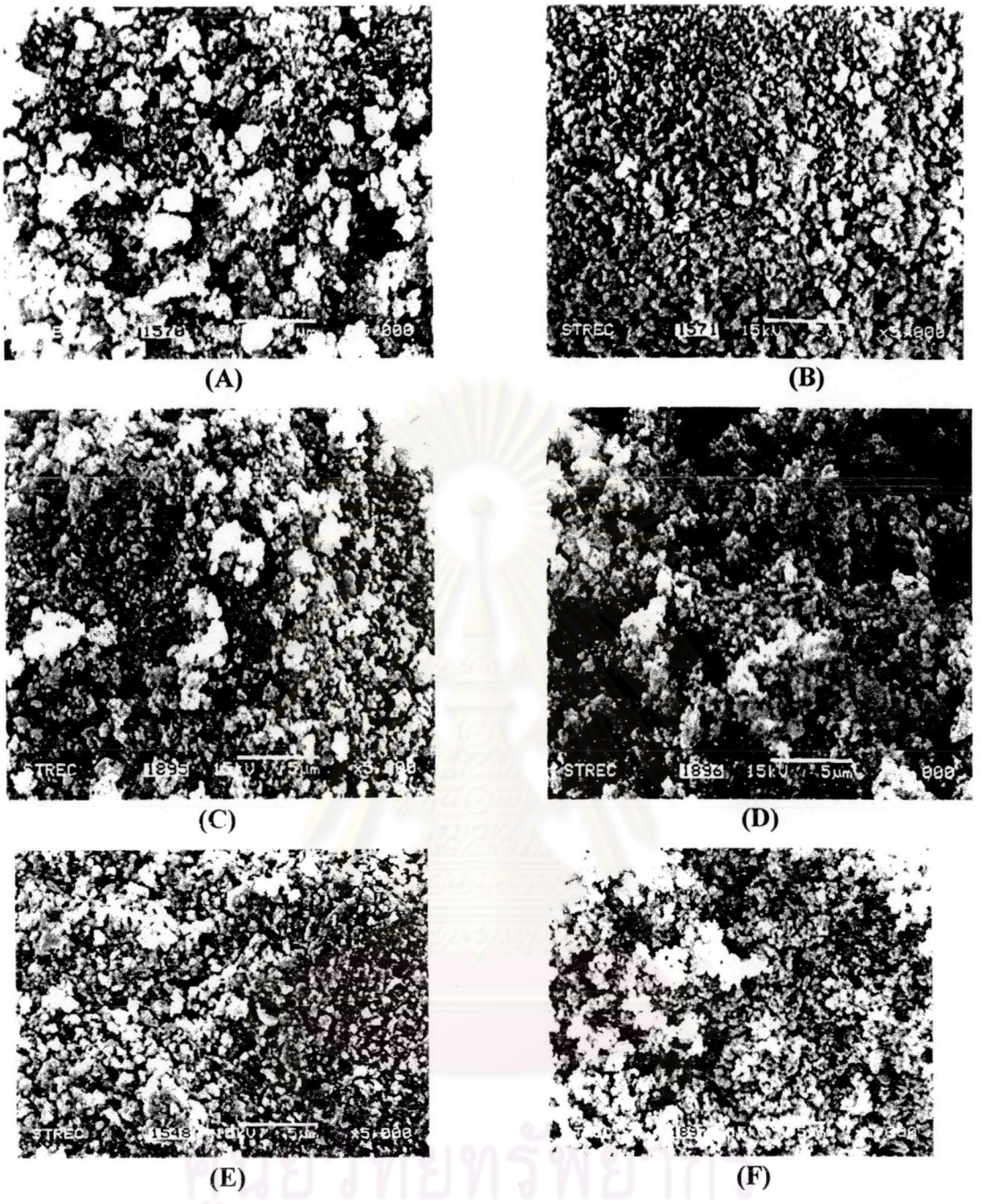


**Figure 5.25** SEM morphology of silicon modified titania products at 340°C. (A) Pure titania, as-synthesized, (B) Pure titania, calcined 900°C, (C) Si/Ti 0.005, as-synthesized, (D) Si/Ti 0.005, calcined 900°C, (E) Si/Ti 0.08, as-synthesized, and (F) Si/Ti 0.08, calcined 900°C.

### 5.3.2 Formation of silicon modified iron (III) oxide

Iron (III) acetylacetonate and an appropriate amount of tetraethyl orthosilicate (TEOS, Si/Fe atomic ratio of 0, 0.005, and 0.08) were added to 100 ml of 1,4-butanediol and heated to a desired temperature (220,and 300°C). The XRD patterns as seen in Figure 5.26 and 5.27, show well defined peaks, clearly assigned to $\gamma$-$Fe_2O_3$. As the Si/Fe ratio increased the crystallite size slightly decreased. The size of the crystallites was calculated using Scherrer's equation, using the most intense diffraction peaks. The $\gamma$-$Fe_2O_3$ crystallites grew with increasing the reaction temperature. On the contrary, the crystallite decreased with increasing the Si/Fe ratio. Table 5.8 present the crystallite size of the as-prepared silicon modified iron (III) oxide and the calcined products at 900°C.

SEM pictures of the as-synthesized silicon modified iron oxide for the reaction temperature of 220°C and 300°C and the products after calcination at 900°C are presented in Figure 5.28 and 5.29 respectively. For the as-synthesized products, SEM images show an irregular and very rough surface. In contrast, with the higher content of Si/Fe charged ratio, SEM picture is characterized by a finer roughness surface. The calcined products provided a lot of globular clusters along with acicular shape bars of $\gamma$-$Fe_2O_3$, indicating that the $\gamma$-$Fe_2O_3$ particles are agglomerated.

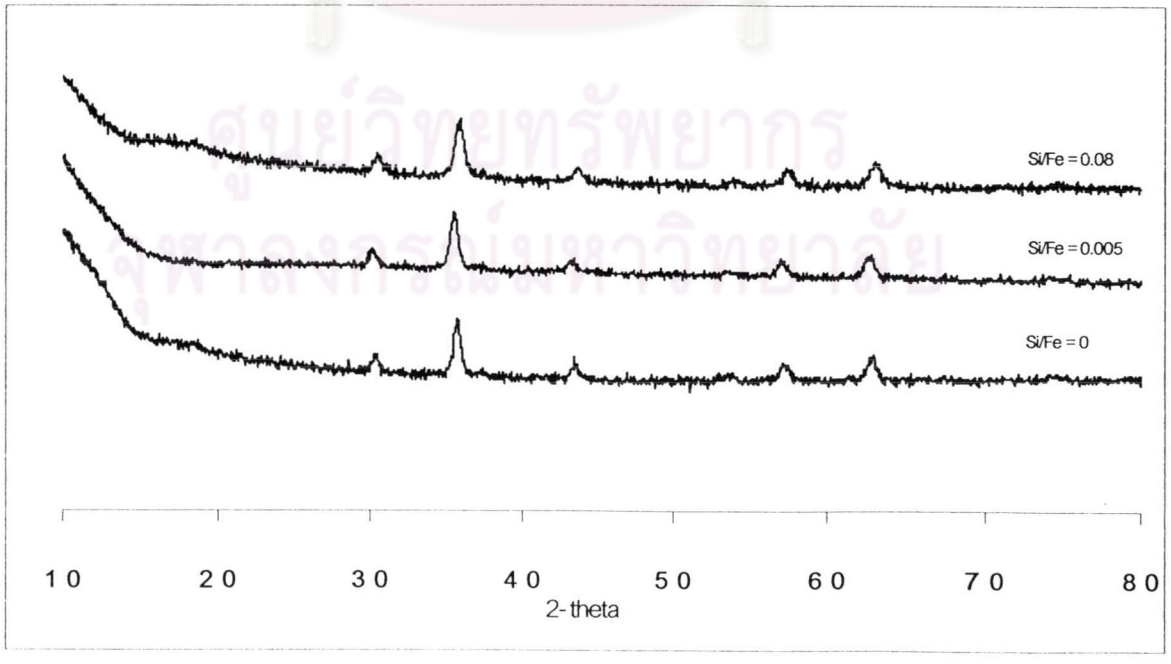


**Figure 5.26** XRD patterns of silicon modified iron (III) oxide for various silicon contents at 220°C

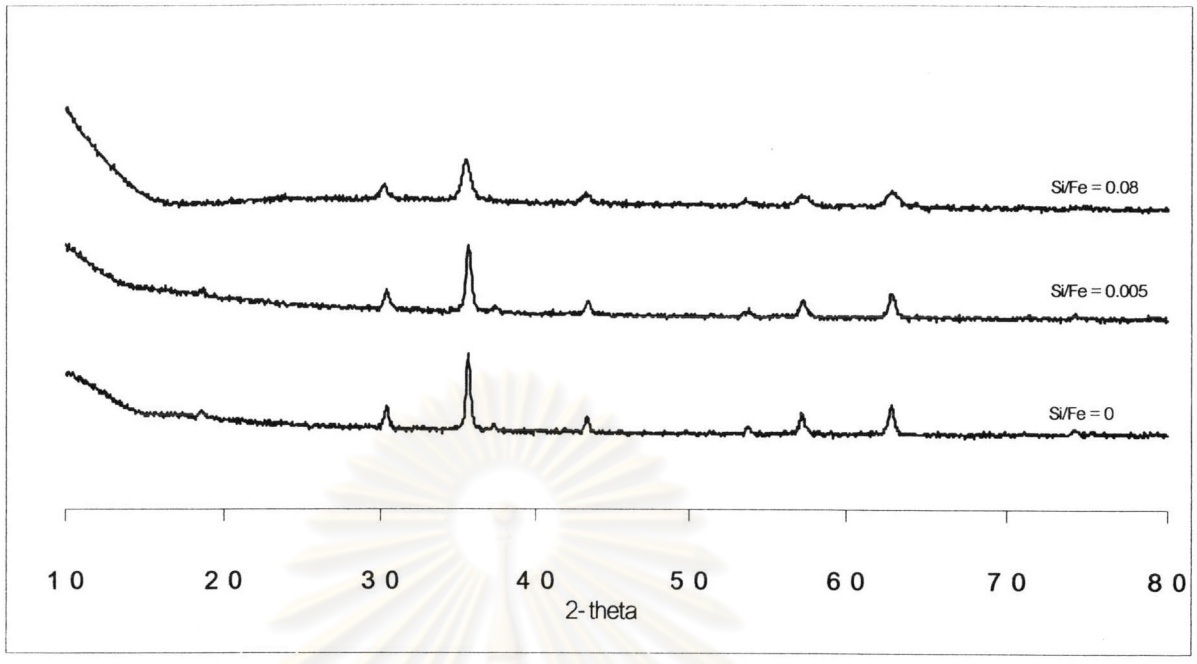


**Figure 5.27** XRD patterns of silicon modified iron (III) oxide for various silicon contents at 300°C

**Table 5.8** Crystallite size data of iron (III) oxide synthesized at various reaction temperature for the different molar ratio of Si/Fe before calcination ($d_0$) and calcined product of 900°C ($d_{900}$)

| Reaction Temperature | Charged Si/Fe ratio | Crystallite size (nm) | | $d_{900}/d_0$ |
|---|---|---|---|---|
| | | $d_0$ | $d_{900}$ | |
| 220 | 0 | 16.6 | 37.5 | 2.3 |
| | 0.005 | 14.5 | 55.3 | 3.8 |
| | 0.08 | 13.3 | 22.9 | 1.7 |
| 300 | 0 | 24.7 | 68.4 | 2.8 |
| | 0.005 | 27.6 | 44.4 | 1.6 |
| | 0.08 | 13.3 | 28.2 | 2.1 |

(A)

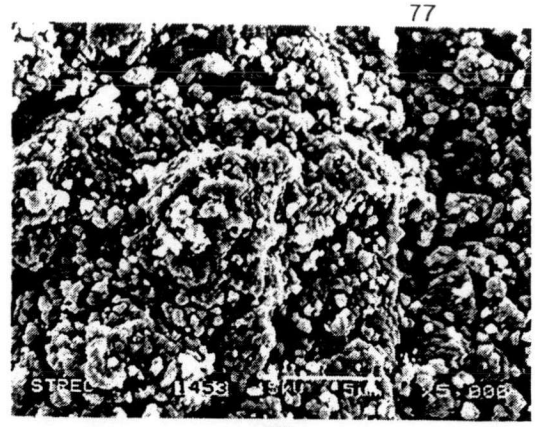

(B)

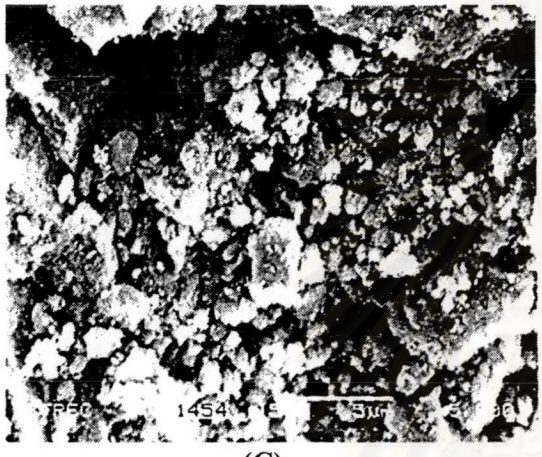

(C)

(D)

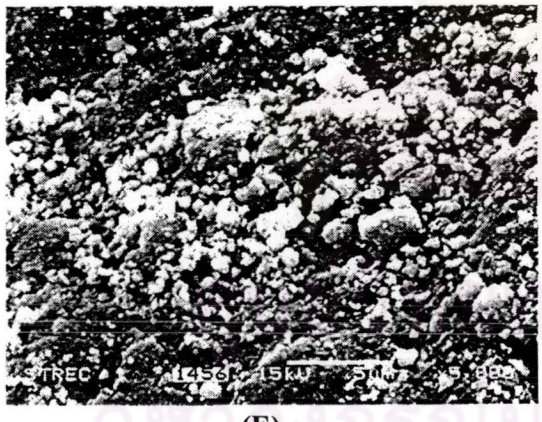

(E)

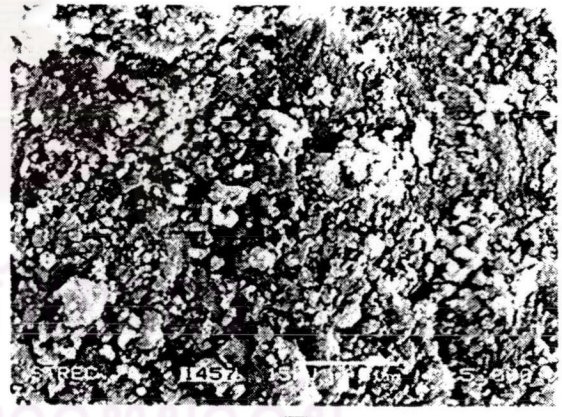

(F)

**Figure 5.28** SEM morphology of silicon modified iron (III) oxide products at 220°C. (A) Pure iron (III) oxide, as-synthesized, (B) Pure iron (III) oxide, calcined 900°C, (C) Si/Fe 0.005, as-synthesized, (D) Si/Fe 0.005, calcined 900°C, (E) Si/Fe 0.08, as-synthesized, and (F) Si/Fe 0.08, calcined 900°C.

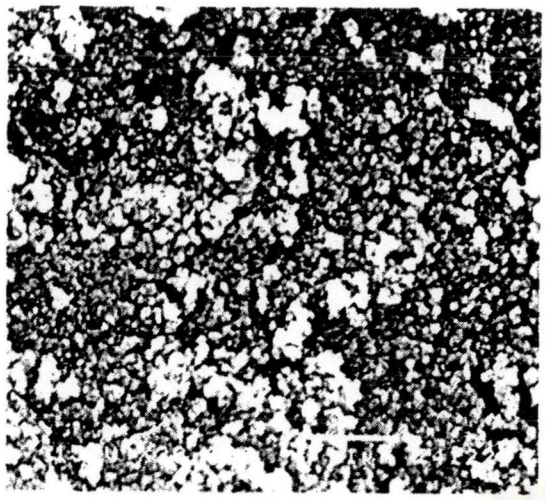

(A)

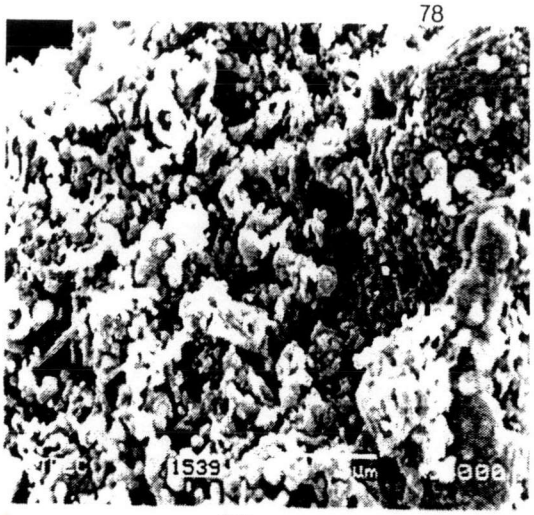


(B)

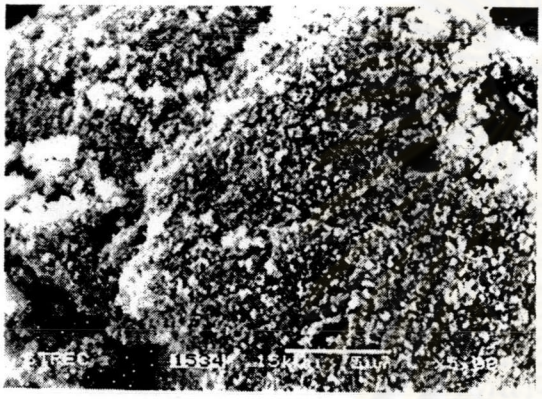

(C)

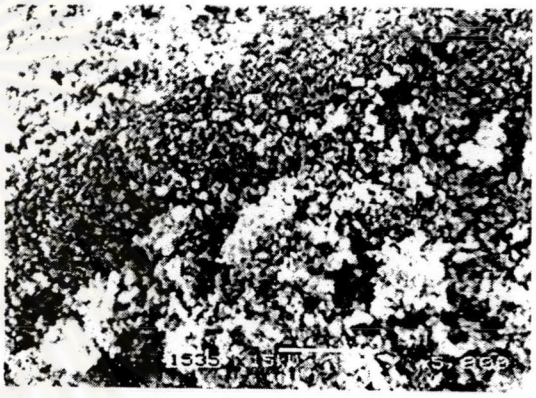


(D)

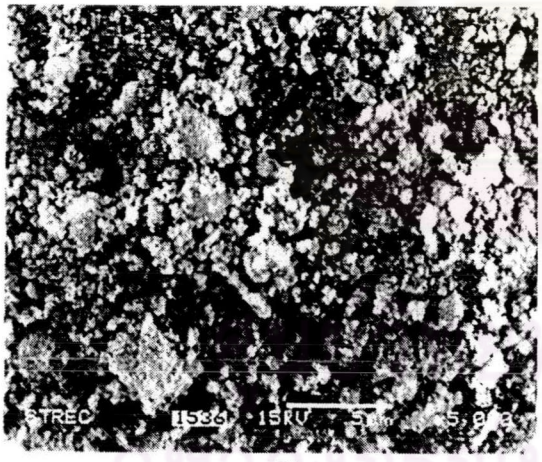


(E)

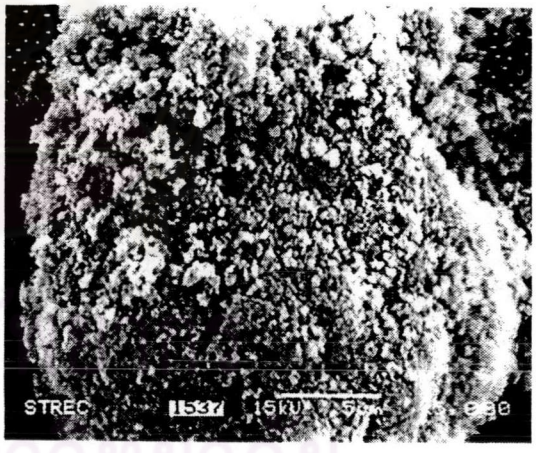


(F)

**Figure 5.29** SEM morphology of silicon modified iron (III) oxide products at 300°C. (A) Pure iron (III) oxide, as-synthesized, (B) Pure iron (III) oxide, calcined 900°C, (C) Si/Fe 0.005, as-synthesized, (D) Si/Fe 0.005, calcined 900°C, (E) Si/Fe 0.08, as-synthesized, and (F) Si/Fe 0.08, calcined 900°C.

### 5.3.3 Formation of silicon modified zinc (II) oxide

The reaction of zinc (II) acetylacetonate and an appropriate amout of tetraethylorthosilicate with the charged ratio Si/Zn of 0, 0.005, and 0.08 in 1,4-butanediol with the reaction temperature varied to 200, and 300°C were done in this work. The typical XRD patterns of the products obtained with the addition of TEOS imply their good crystallinity. All diffraction peaks in the XRD patterns of the as-synthesized ZnO can be assigned to the hexagonal structure and the peak intensities were not affected by the TEOS content in the reaction mixture as seen in Figure 5.30 and 5.31 respectively. The crystallite size of the as-prepared silicon modified zinc (II) oxide and the calcined product at 900°C are concluded in Table 5.9, which the crystallite size decreased with increasing the Si/Zn charged ratio.

The SEM image of the as-synthesized silicon modified zinc (II) oxide and the calcined products at 900°C are presented in Figure 5.32 and 5.33. It is observed that for the reaction temperature was 200°C the particles exhibit the lumpy surface. When the reaction temperature was 300°C, observed the particle with a rod-like shape with increasing the amount of silicon content to Si/Zn molar ratio of 0.08 the SEM image presented the prismatic-like of the product after calcination at 900°C.

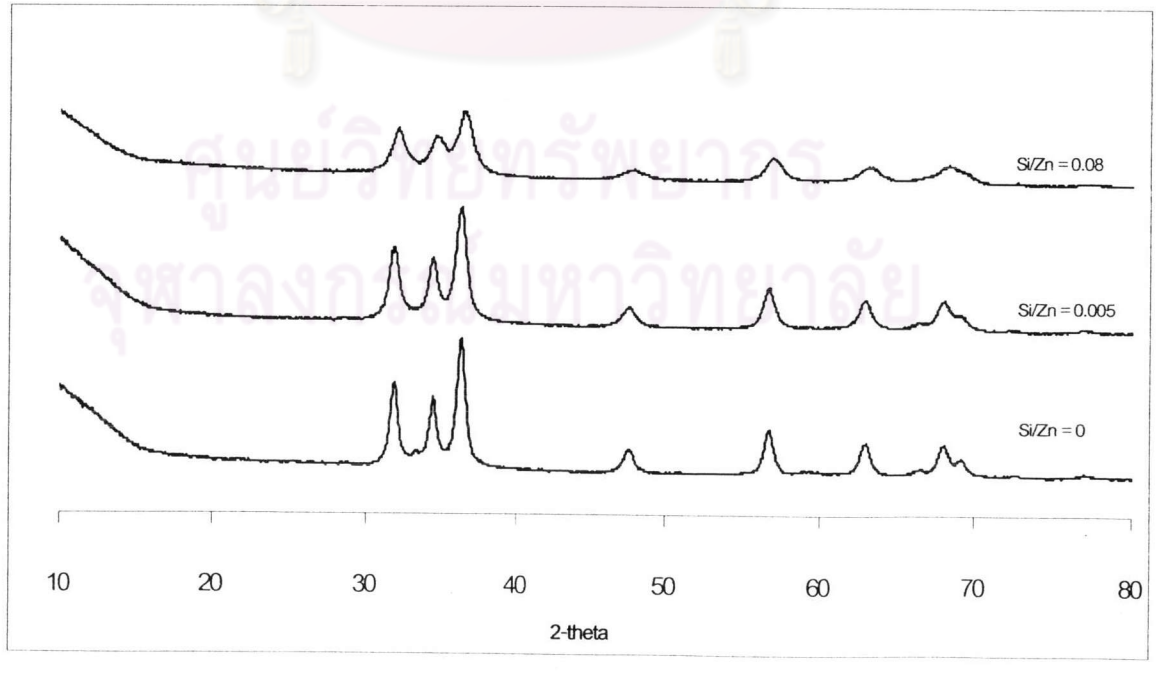


**Figure 5.30** XRD patterns of silicon modified zinc (II) oxide for various silicon contents at 200°C

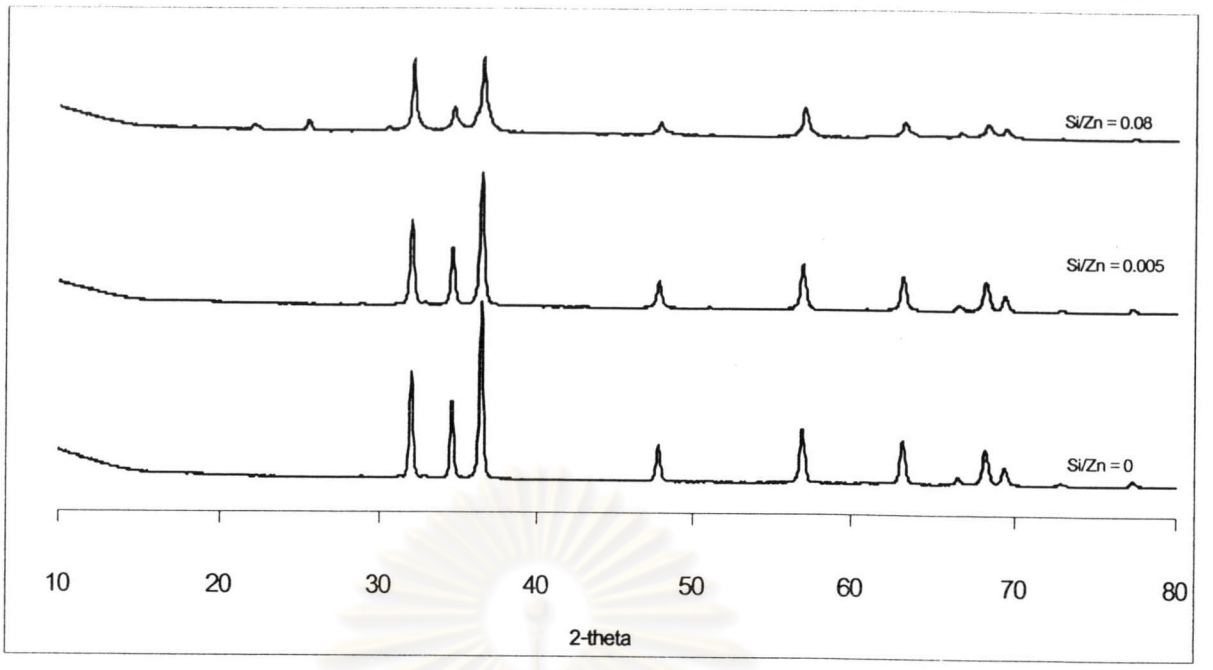


**Figure 5.31** XRD patterns of silicon modified zinc (II) oxide for various silicon contents at 300°C

**Table 5.9** Crystallite size data of zinc (II) oxide synthesized at various reaction temperatures for the different molar ratio of Si/Zn before calcination ($d_0$) and calcined product of 900°C ($d_{900}$)

| Reaction Temperature (°C) | Charged Si/Zn ratio | Crystallite size (nm) | | $d_{900}/d_0$ |
|---|---|---|---|---|
| | | $d_0$ | $d_{900}$ | |
| 200 | 0 | 14.3 | 146.1 | 10.2 |
| | 0.005 | 12.1 | 64.0 | 5.3 |
| | 0.08 | 7.9 | 31.0 | 3.9 |
| 300 | 0 | 68.9 | 156.6 | 2.3 |
| | 0.005 | 53.2 | 139.2 | 2.6 |
| | 0.08 | 38.1 | 43.6 | 1.1 |

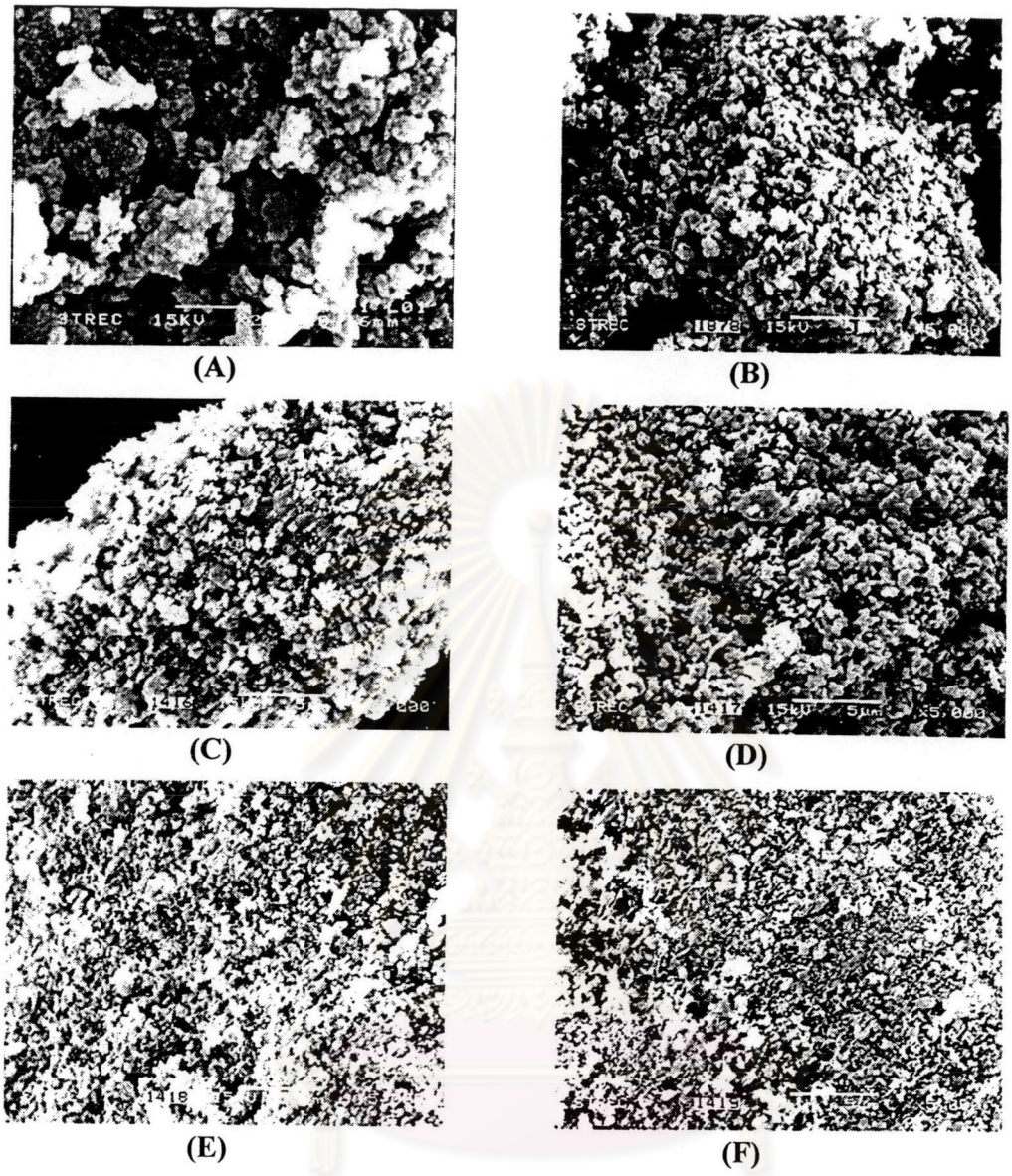


**Figure 5.32** SEM morphology of silicon modified zinc (II) oxide products at 200°C. (A) Pure zinc (II) oxide, as-synthesized, (B) Pure zinc (II) oxide, calcined 900°C, (C) Si/Zn 0.005, as-synthesized, (D) Si/Zn 0.005, calcined 900°C, (E) Si/Zn 0.08, as-synthesized, and (F) Si/Zn 0.08, calcined 900°C.

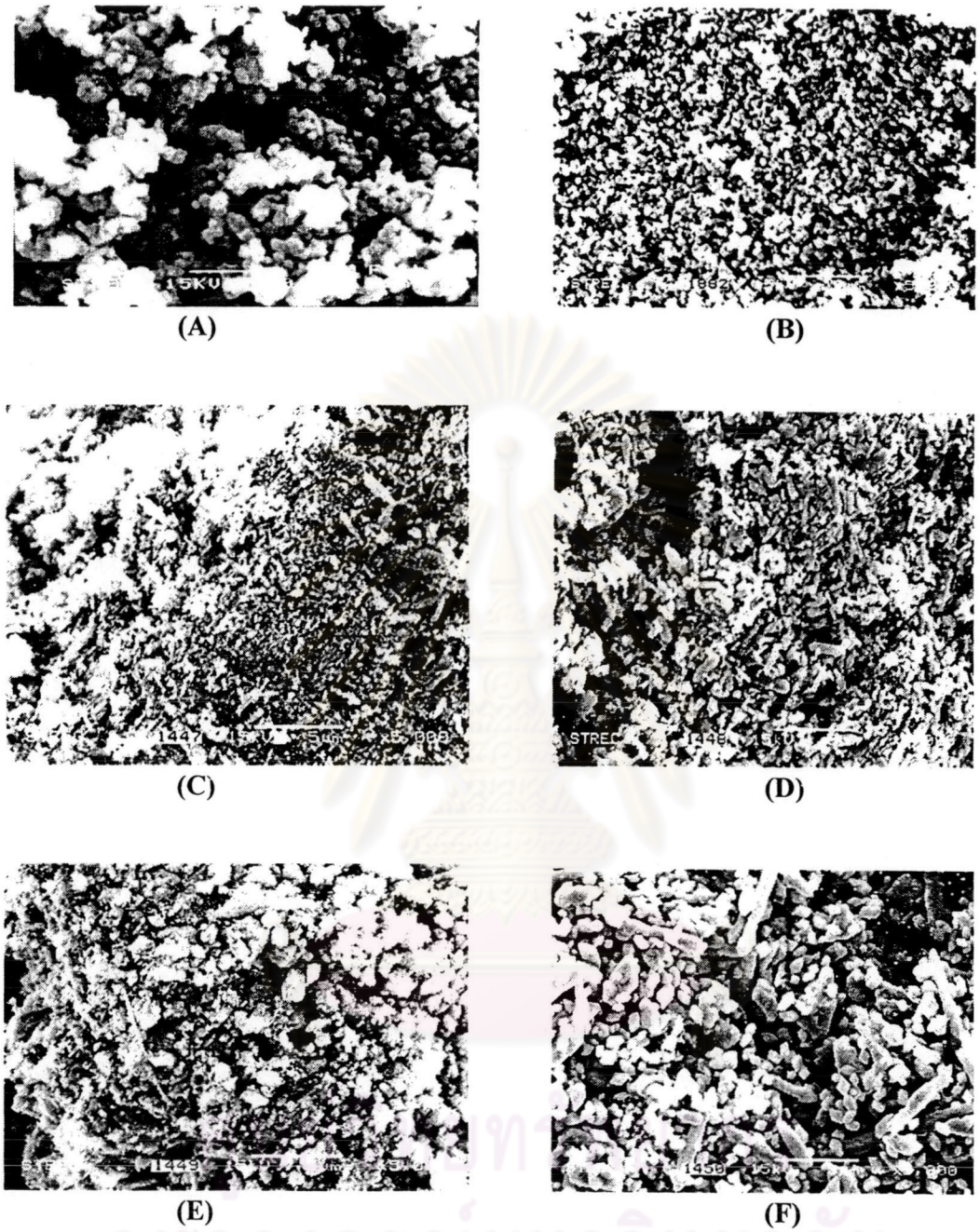


**Figure 5.33** SEM morphology of silicon modified zinc (II) oxide products at 300°C. (A) Pure zinc (II) oxide, as-synthesized, (B) Pure zinc (II) oxide, calcined 900°C, (C) Si/Zn 0.005, as-synthesized, (D) Si/Zn 0.005, calcined 900°C, (E) Si/Zn 0.08, as-synthesized, and (F) Si/Zn 0.08, calcined 900°C.



## 5.4 Effects of silicon on the crystallite size of metal oxide product

### 5.4.1 Effects of silicon on the crystallite size of titanium (IV) oxide

Apparently as seen from Figure 5.34, the small crystal size synthesized at low temperature and the large size at the reaction temperature higher than 300°C for undoped titania. For small as-synthesized crystal, doping a small amount of silicon the reduction of crystal size does not change much. This result are the same for large as-synthesized crystal. When doping more silicon (8%), the decrease of crystal apparently occur for large crystal size.

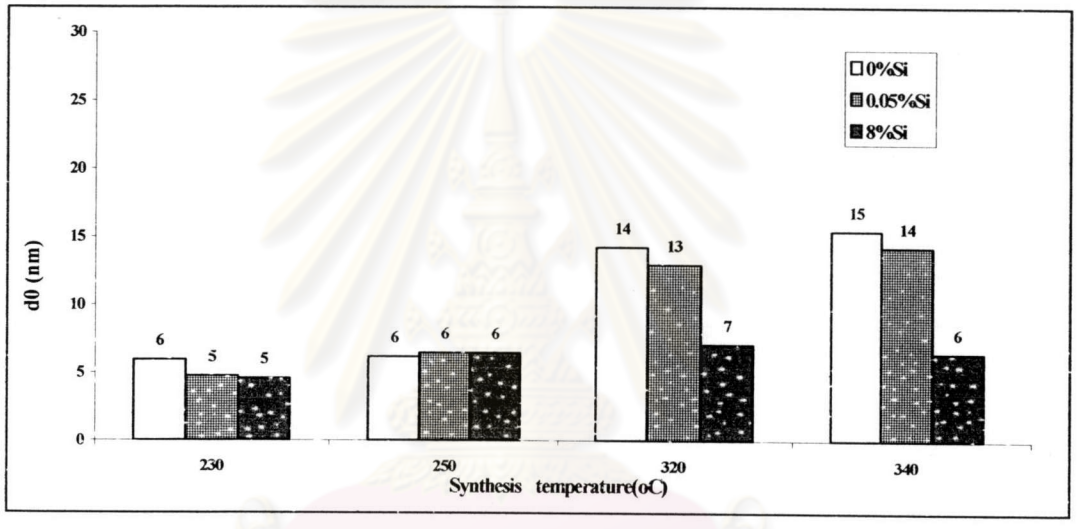


**Figure 5.34** Effects of %Si on the reduction of crystal size of titanium (IV) oxide

### 5.4.2 Effects of silicon on the crystallite size of iron (III) oxide

The effects of silicon on the reduction of as-synthesized crystal are presented in Figure 5.35. The small crystal size of undoped sample does not change much when the percentage of silicon doped was varied. In the contrary, the large in crystal size play in an opposite role that is the crystal gradually decreased when doped for more percentage of silicon.

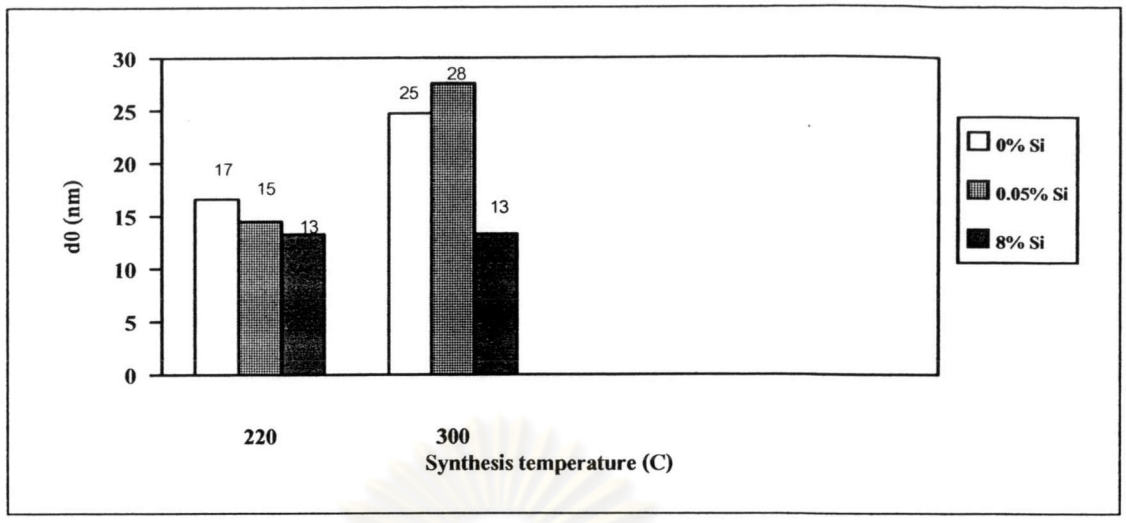


**Figure 5.35** Effects of %Si on the reduction of crystal size of iron (III) oxide

### 5.4.3 Effects of silicon on the crystallite size of zinc (II) oxide

Figure 5.36 show the effects of silicon on the nanocrystallite zinc(II) oxide. The effect of silicon on the reduction of undoped crystal does not change much. The reduction of small crystal size of undoped sample does not affected by varied the percentage of silicon doped. On the other hand, for large crystallite size exhibited more decreasing.

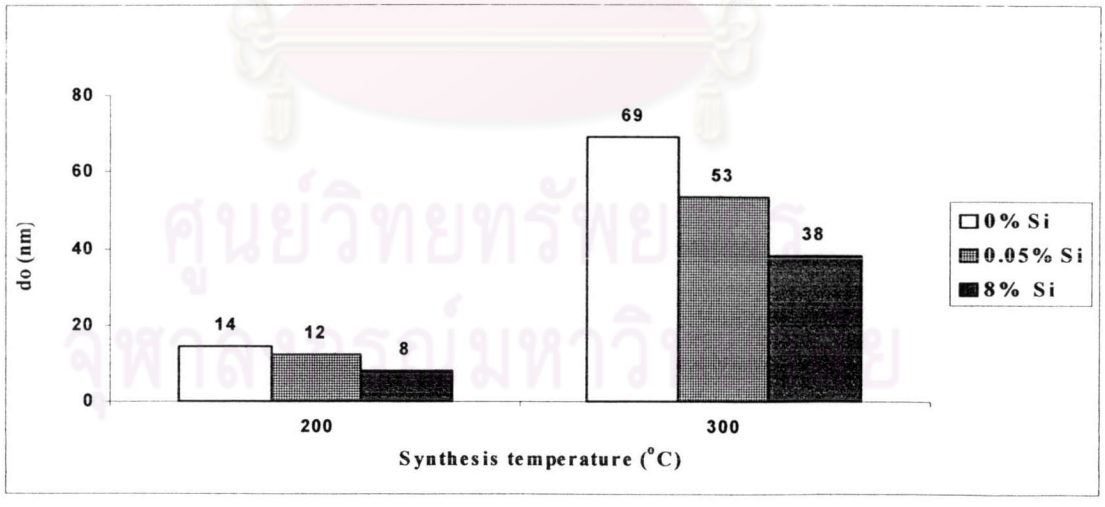


**Figure 5.36** Effects of %Si on the reduction of crystal size of zinc (II) oxide

## 5.5 Effects of silicon on the thermal stability of metal oxide products

To determine the thermal stability of metal oxide, the crystallite size data of the products were plotted as the relation between $d_{900}/d_0$ versus $d_0$. From this relation the thermal stability can be defined as,

$$\text{Thermal stability} = d_{900}/d_0$$

Where $d_{900}$ = crystallite size of product after calcined at 900°C

$d_0$ = as-synthesized crystallite size

The crystallite size is subjected to change after calcination. The product with higher thermal stability would be the least change in crystallite size.

### 5.5.1 Effects of silicon on the thermal stability of titanium (IV) oxide

The effect of silicon on the thermal stability are presented in Figure 5.37 as the crystal growth from sintering. For the small size of as-synthesized crystal, the crystal growth is quite high. When varied the percentage of silicon added to 0.05 and 8%, respectively. It retarded a growth rate of sintering as much as increase silicon. On the other hand, for large as-synthesized crystal size the addition of silicon is negligible. Size of crystal after calcined at 900°C does not change much when adding silicon compared to the small as-synthesized crystal size.

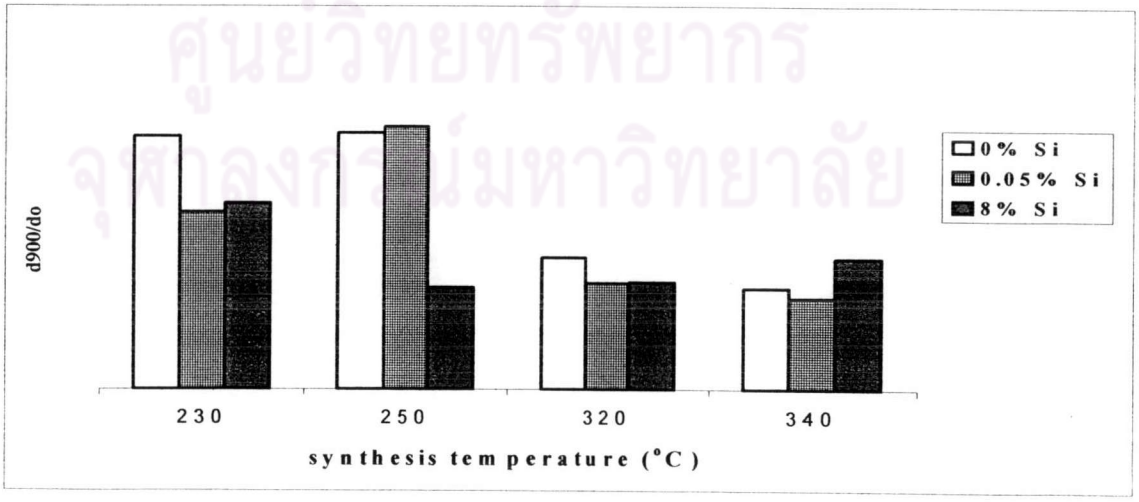


**Figure 5.37** Effects of %Si on the thermal stability of titanium (IV) oxide

### 5.5.2 Effects of silicon on the thermal stability of iron(III) oxide

Figure 5.38 presented the effects of silicon on the thermal stability of iron (III) oxide. Comparison between small and large crystallite size. Doping silicon to the small crystal, the crystal growth gradually increased when added more silicon, the crystal growth drastically decreased. Considering large crystal, adding silicon resulted in the slightly decreased in crystal growth.

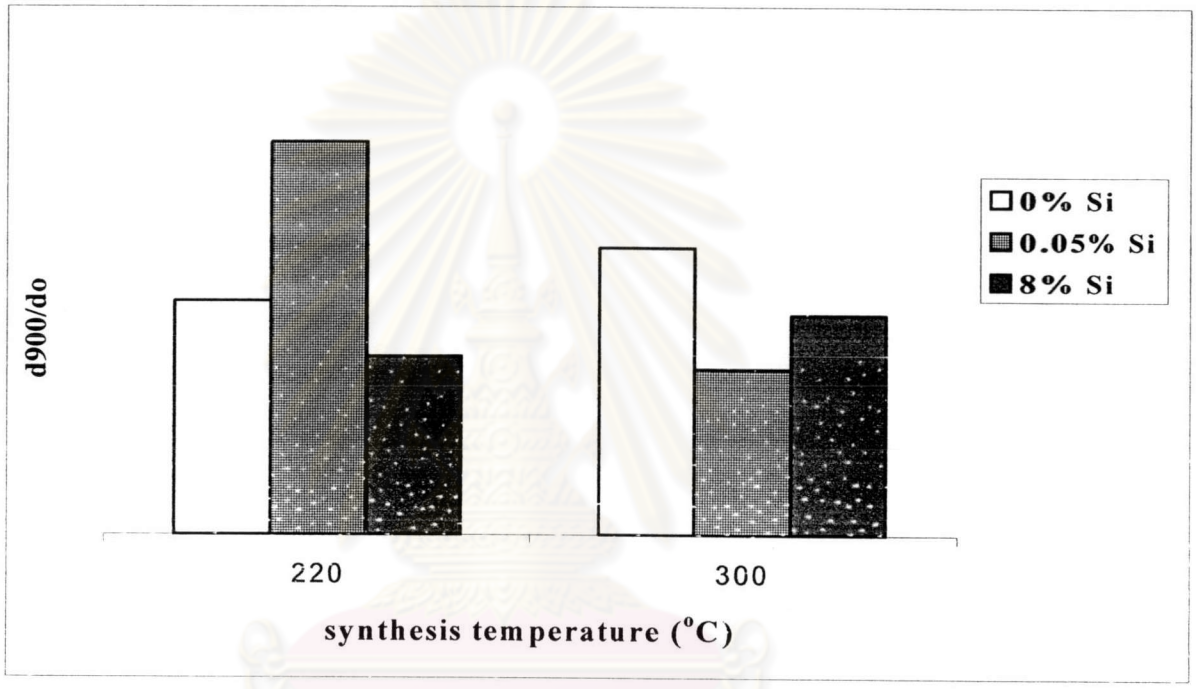


**Figure 5.38** Effects of %Si on the thermal stability of iron (III) oxide

### 5.5.3 Effects of silicon on the thermal stability of zinc (II) oxide

The effects of silicon on the thermal stability of zinc (II) oxide are presented in Figure 5.39. For the small crystallite size, the crystal growth is quite high. When adding silicon, the crystal growth drastically decreased. It retarded a growth rate of sintering as much as increased silicon. On the contrary, for large as-synthesized crystal, the addition of silicon is not affected. The crystallite size after the calcination does not change much when adding silicon compared to the small size.

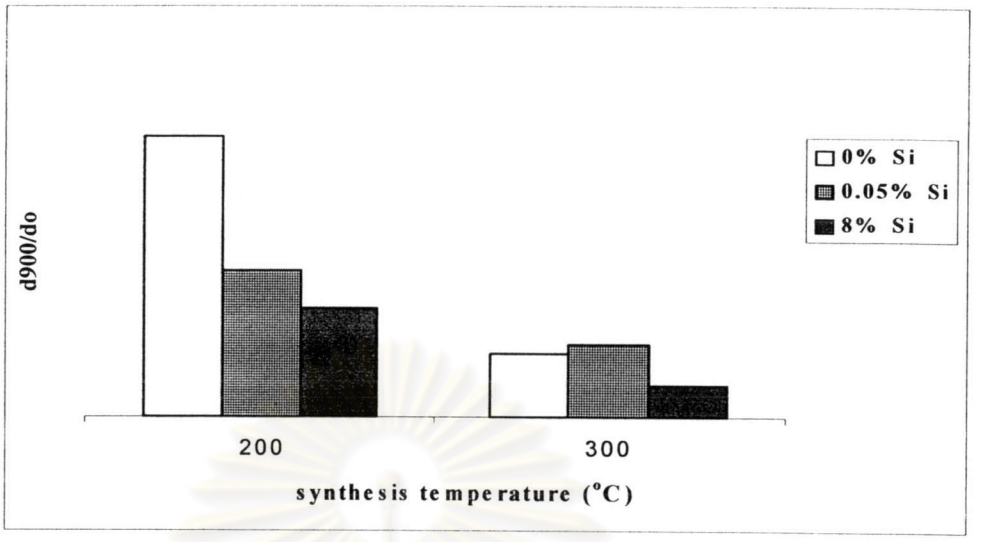


**Figure 5.39** Effects of %Si on the thermal stability of zinc (II) oxide